Preparation of tripodal Vanadium Oxo-Organometallic Species Supported on Silica, [(≡SiO) 3 V(O)], for Selective Non-Oxidative Dehydrogenation of Propane

Jessy Abou Nakad, Remy Rajapaksha, Kai Chung Szeto, Aimery De mallmann, Mostafa Taoufik

Preparation of tripodal Vanadium Oxo-Organometallic Species Supported on Silica, [(≡SiO)$_3$V(=O)], for Selective Non-Oxidative Dehydrogenation of Propane

Jessy Abou Nakad,[a] Remy Rajapaksha,[a] Kai C. Szeto,[a] Aimery De Mallmann,[a] Mostafa Taoufik[a,*]

[a] Université Lyon 1, Institut de Chimie Lyon, CPE Lyon, CNRS, UMR 5128 CP2M, 43 Bd du 11 Novembre 1918, F-69616 Villeurbanne Cedex, France. E-mail: Mostafa.Taoufik@univ-lyon1.fr; Fax: +33 (0)472 431 798; Tel: +33 (0)472 431 795

Abstract.

In this work, a strategy based on the grafting of a vanadium molecular complex, [V(=O)(O*t*Bu)$_3$], **(1)**, bearing tert-butoxide ligands, on a partially dehydroxylated silica, followed by a thermal treatment has been used for the preparation of supported tripodal V oxo complex, [(≡SiO)$_3$V(=O)], active species, for important chemical processes. The molecular complex reacts with a silica partially dehydroxylated at 200 °C ($SiO_{2\text{-}200}$) to lead to bipodal [(≡SiO)$_2$V(=O)(O*t*Bu)] **(2)** as major surface species, while monopodal surface species [(≡SiO)V(=O)(O*t*Bu)$_2$] **(3)** are obtained on $SiO_{2\text{-}700}$. These materials were thermally treated to form active supported tripodal vanadium oxo species by releasing isobutene via a β-H transfer, leading to V-OH intermediate. The latter species lead to the targeted tripodal oxo species [(≡SiO)$_3$V(=O)] after restructuration of the support and will be represented as materials **(2a)** and **(3a)**. All the supported vanadium complexes were characterized by DRIFT, UV-Vis, solid-state NMR and XANES spectroscopies. In particular, the structure of isolated vanadium oxo tripodal species, [(≡SiO)$_3$V(=O)], was confirmed by ^{51}V NMR with a major peak at -670 ppm, as reported in literature. The catalytic property of **(2a)** and **(3a)** were evaluated for the direct propane dehydrogenation and showed promising performances that can be solely assigned to the isolated vanadium tripodal species.

Introduction

Propylene is an important intermediate in the chemical industry and is used for the synthesis of several key products such as polypropylene, acrylonitrile and propylene oxide.[1,2] It is mainly produced by steam cracking (SC) and fluid catalytic cracking (FCC) of hydrocarbon feedstocks.[1,3]. With the increasing demand for propylene globally, SC and FCC will be unable to satisfy the market need. Hence, alternative routes such as on-purpose technologies have been developed, like olefin metathesis,[4–6] methanol to olefin process,[7] and more recently, the direct CO_2 conversion to light olefins[8,9] as well as catalytic propane dehydrogenation.[1,10] The latter uses catalysts that can operate under oxidative or non-oxidative conditions. The main issue of the oxidative dehydrogenation is the low selectivity to olefins as CO_2 can easily be produced from a total oxidation of light hydrocarbons. Non-oxidative dehydrogenation of propane (PDH) is widely used at industrial scale as it offers many advantages, such as a high selectivity toward the desired alkene (propylene) and the production of valuable dihydrogen. This reaction is highly endothermic ($\Delta H° = 124$ kJ·mol^{-1}) and requires high operating temperatures (above 550 °C), resulting in undesired side-reactions (cracking) and deactivation of the catalyst due to the formation of coke and degradation/restructuration of the active phase. Two PDH processes dominate the market, known as Oleflex® and Catofin®. The first one employs supported hetero-bimetallic particles based on a noble metal Pt, alloyed with toxic Sn as a promoter, to enhance the selectivity to propylene, and to avoid cracking reactions and the fast deactivation of the catalyst at high temperature. However, despite the presence of promoters, high operating temperatures lead to a slow deactivation as a function of time on stream, which requires frequent regeneration treatments in order to maintain the catalytic performances. The Catofin® technology employs a cheap catalyst based on chromium oxides (typically 18-20 wt% Cr) supported on alumina with working temperatures ranging from 575 to 625 °C at reduced pressures (0.2 to 0.5 bar). The high temperature required to improve catalytic activity toward the desired product, leads inevitably to the formation of coke. Consequently, the regeneration cycles occurring every 15-30 min, decrease the activity, and therefore a replacement of the catalyst every two years is needed. In addition to coke formation, the process conditions lead to aging of the catalyst. This causes: i) a decrease of the dispersion of chromium species on the surface; ii) an incorporation of the Cr active species within alumina, resulting in an increase of the catalyst's acidity that reduces propylene selectivity; iii) an increase of the surface Cr^{6+}/Cr^{3+} ratio after each regeneration cycle by calcination.[11]

To overcome these challenges, other metal oxides such as VO_x, GaO_x, InO_x or MoO_x have been widely explored in the literature for PDH.[1] Supported vanadium oxides catalysts have been intensively studied for the oxidative dehydrogenation of propane and showed promising results, while few examples were reported in the case of the non-oxidative propane dehydrogenation. Vanadium(V) oxide supported on

silica, alumina or titanium oxide shows promising activities for the catalytic dehydrogenation of light alkane.[12–17] The conventional synthesis methods of these catalysts described in literature involve various processes such as aqueous impregnation, sol-gel, chemical vapor deposition, to name a few.[1] However, depending on the nature of the vanadium precursor and the support used, these synthesis methods of supported vanadium oxo complexes, lead to a distribution of monomeric, dimeric and oligomeric VO_x species on the surface or even to particles of oxide.[18,19] Several studies in this area have been reported and suggest that the structure of the supported precursor of the active species, for example onto silica, is postulated as an isolated vanadium center bearing an oxo and three siloxy ligands. In the case of vanadium systems, it is reasonable to propose that the active species is V^{3+} trisiloxy (Scheme 1) obtained during the initiation step, after an activation of propane on V^{5+} oxo tripodal species[20], similar to chromium and gallium catalytic systems.

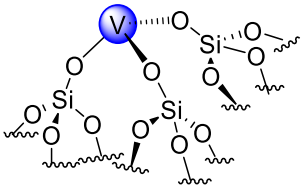

Scheme 1. Proposed tripodal $V^{(III)}$ active species for PDH

Based on DFT calculations and Operando studies, the mechanism of propane dehydrogenation in the case of metal oxides has been proposed to occur via a heterolytic C-H bond cleavage via activation on a surface M-O- bond, leading to a coordinated alkyl, M-R and a surface hydroxyl, -OH or via a σ-bond metathesis on a M-H intermediate.[1,21] The low concentration of active sites hampers their characterization and thus limited information is available on their role in catalysis and the understanding of the elementary steps. In fact, many attempts to characterize the surface-active sites of supported VO_x species, prepared by conventional methods, using spectroscopic techniques for bulk systems such as XAFS and ^{51}V MAS-NMR led to inconsistent results.[22–29] An obvious strategy to access to the real model of the active species and to increase the activity in PDH, is to control the number of active sites and to eliminate presumably inactive oligomeric VO_x sites. Regarding the preparation of well-defined functional materials at a molecular scale, especially single-site catalysts for PDH, surface organometallic chemistry has proven to be a powerful approach. This methodology involves a controlled grafting of a reactive organometallic precursor on a pretreated support. With a judicious choice of the precursor in combination with the pre-treatment of the support, supported species with a desired podality, oxidation state and coordination environment around the metal center can be designed.[30] This approach has resulted in highly active catalysts associated with the propylene chemistry, mainly through olefin metathesis, [4–6,31–38] but also for PDH.[39–45] Therefore, we intend to

apply surface organometallic chemistry for the synthesis of a silica material containing supported trisiloxy vanadium oxo species as pre-catalyst for propane dehydrogenation reaction. We recently developed a new synthetic method for the preparation of supported active sites, by using a molecular complex of group VI bearing tert-butoxide ligands [M(=O)(O*t*Bu)$_4$] (M = Mo or W). After a grafting reaction of these complexes onto silica followed by a thermolysis, [(≡SiO)$_2$M(=O)$_2$] species were obtained and showed high activities for the metathetic oxidation or the metathesis of olefins.[46,47] In the case of vanadium, we expect that this strategy would result in the formation of a well-defined tripodal vanadium oxo species after the grafting of [V(=O)(O*t*Bu)$_3$], **(1)**, onto silica supports (dehydroxylated at 200 and 700 °C). A thermal treatment at high temperature of the resulting surface species, bearing one or two tert-butoxide ligands, leads to the targeted active species by a β-H elimination of isobutene from V-O*t*Bu, resulting in a hydroxy ligand σ-coordinated to vanadium, V-OH. This reaction can be followed by a ring opening of a neighboring siloxane (≡Si-O-Si≡) which forms a new V-OSi≡ bond and a surface hydroxyl group, ≡Si-OH. These well-defined surface species have been further characterized by elemental analysis and different spectroscopic techniques such as DRIFT, solid state NMR of different nuclei (^{1}H, ^{13}C, ^{51}V), UV-Vis, XAS and studied as catalysts for the non-oxidative dehydrogenation of propane in a continuous flow reactor.

Experimental Section

General Procedure.

All experiments were carried out using standard air-free methodology within an argon-filled glovebox, on a Schlenk line or in a Schlenk-type apparatus interfaced to a high-vacuum line (10^{-5} mbar). Solvents were purified and dried according to standard procedures. [V(=O)(O*t*Bu)$_3$] was synthesized in one step followed by purification. Elemental analyses were performed at Mikroanalytisches Labor Pascher. Diffuse reflectance infrared spectra were collected with a Nicolet 6700 FT-IR spectrophotometer, in 4 cm^{-1} resolution with a SMART module. An air-tight IR cell equipped with CaF_2 windows was employed and the final spectra comprise 64 scans. Diffuse reflectance UV-Vis spectra in the range of 200-850 nm were recorded on a Perkin Elmer λ1050 UV-Vis-NIR spectrophotometer adapted with the Praying Mantis optical unit provided by Harrick. The samples were diluted in dry $BaSO_4$ and the spectra were recorded against a $BaSO_4$ baseline. An air-tight cell equipped with quartz windows was used.

Solution NMR spectra were recorded on an Avance-300 Bruker spectrometer. All chemical shifts were measured relative to residual ^{1}H or ^{13}C resonance of the deuterated C_6D_6 solvent: δ 7.15 ppm for ^{1}H and 128 ppm for ^{13}C. Solid-state NMR spectra were acquired with a Bruker Avance 500 spectrometer

(^{1}H: 500.1 MHz, ^{13}C: 125.7 MHz). For ^{1}H experiments, the spinning frequency was 10 kHz, the recycle delay was 5 s and 8 scans were collected using a 90° pulse excitation of 3 μs. The ^{13}C CP MAS spectra were obtained at a spinning frequency of 10 kHz, with a recycle delay of 5 s and 12288 scans were collected. Chemical shifts were given in ppm with respect to TMS as external reference for ^{1}H and ^{13}C NMR. The ^{51}V MAS NMR spectrum was acquired in a Bruker DSX 300 spectrometer (^{51}V: 78.9 MHz) using a single pulse excitation. The signal was optimized with crystalline V_2O_5 (δ= - 609 ppm) as external standard with a pulse angle of π/2. Two spinning rates were used in order to determine the isotropic chemical shift (10 kHz and 12 kHz).

X-ray absorption spectra were acquired at ESRF on BM23 beam-line, at room temperature at the vanadium K edge. A double Si(111) crystal was used as monochromator and a system based on a total reflection through a double X-ray mirror with an incidence angle variable from 2 to 5 mrad allowed harmonic rejection to a level better than 10^{-5}.[48] The spectra were recorded in the transmission mode between 5.3 to 6.44 KeV at room temperature (295 K). Each data set was collected simultaneously with a V metal foil reference and was later aligned according to that reference (first maximum of the derivative of the V foil spectrum set at 5465.1 eV). The molecular complexes and vanadyl sulfate were homogeneously mixed with dry BN and the supported V samples were packaged as pellets within an argon filled glove-box in a double air-tight sample holder equipped with kapton windows. The data analyses were performed by standard procedures using in particular the program "Athena".[49]

Preparation of the complex:

The vanadium precursor [V(=O)(O*t*Bu)$_3$], **(1)**, was synthesized by the reaction of V_2O_5 (Aldrich) with *t*BuOH in benzene. The entire preparation procedure was carried out in an inert atmosphere using a Schlenk line. 20 grams of V_2O_5 was first placed in a 1-L round-bottom flask and connected to a Dean–Stark trap in order to capture the water from the reaction, coming through the reflux condenser. After adding 300-mL of dry benzene, 165 ml of dry *t*BuOH was added to the benzene suspension of V_2O_5. The temperature was increased to 100 °C and maintained for 48 hours. The solution was filtered away from unreacted V_2O_5. After removing the solvent by distillation, white crystals were observed. This product was further dried overnight under reduced pressure. In order to purify the freshly formed product, [V(=O)(O*t*Bu)$_3$], a sublimation was conducted under vacuum at 40 °C. ^{1}H NMR (C_6D_6): δ=1.43 ppm (C*H*$_3$); ^{13}C{H} NMR (C_6D_6) δ= 31.4 ppm (*C*H$_3$) and 86 ppm (*C*-CH$_3$).

Preparation and characterization of (2), (2a), (3) and (3a) materials.

A mixture of [V(=O)(O*t*Bu)$_3$] (in excess with respect to total amount of Si-OH groups, 0.6 g in this case) and $SiO_{2-(200)}$ (2 g) in pentane (10 mL) was stirred at 25 °C for 4 hours. After filtration, the solid was washed 4 times with pentane and the liquid was transferred into another reactor in order to quantify the *t*BuOH evolved during the grafting reaction by GC and using an internal standard. The resulting

material, **(2)**, is a white powder that was dried under vacuum (10^{-5} mbar). Elemental analysis: V 1.6 wt% C 1.5 wt%. The catalyst was characterized by DRIFT, Solid-State NMR, UV-Vis and XANES.
The same procedure was employed with $SiO_{2\text{-}700}$ to yield **(3)**, which was also characterized as **(2)**. Elemental analysis: V 1.12 wt%, C 2.23 wt%.
Both materials, **(2)** and (**3)** were heated to form tripodal V species leading to the synthesis of **(2a)** and **(3a)** materials, respectively. These species were characterized by DRIFT, Solid-State NMR UV-Vis, and XANES and their catalytic performances evaluated for propane dehydrogenation.

Catalysts evaluation. Catalytic propane conversion was carried out in a stainless-steel continuous flow reactor (P_{total} = 1 bar, T = 540 °C, total flow rate = 5 mL.min^{-1}: 20% propane in argon; mass of the catalyst = 500 mg diluted in 2.5 of CSi). The gases were purified with a column of molecular sieves and activated Cu_2O/Al_2O_3 and controlled by Brooks mass flow controllers. The catalyst was charged in the glovebox. A 4-way valve allowed the isolation of the charged catalyst in the reactor from the environment and extensive purging of the tubes before the reaction. The products were determined by an online HP 6890 GC equipped with a 50 m KCl/Al_2O_3 column and a FID detector.

Results and Discussions

Preparation and characterization of [V(=O)(O*t*Bu)$_3$], (1)

The precursor, [V(=O)(O*t*Bu)$_3$], was easily synthesized using commercially available compounds V_2O_5 and *t*BuOH in benzene at 100 °C for 48 h. After purification, this complex was identified by intense ^{1}H NMR signal at 1.43 ppm, attributed to proton of methyl fragments and ^{13}C NMR signals at 31.4 ppm, corresponding to carbons of methyl groups, **C**H$_3$, and at 86 ppm attributed to the quaternary C of the tert-butyl ligand (Figure S1). In addition, ^{51}V NMR showed a signal at – 642 ppm, corresponding to a tetrahedral vanadium supported complex, bearing an oxo and three alkoxy ligands (Figure S2).[42]

Reactivity of [V(=O)(O*t*Bu)$_3$], (1),with a silica dehydroxylated at 200 °C, synthesis of material (2)

Amorphous silica, Aerosil 200 from Degussa was partially dehydroxylated at 200 °C under high vacuum (10^{-5} mbar) to afford $SiO_{2\text{-}200}$ with a density of silanols ca. 2.5 OH per nm^2 (0.86 mmol OH.g^{-1}).[40] The grafting of [V(=O)(O*t*Bu)$_3$] on $SiO_{2\text{–}200}$ was carried out by an anhydrous impregnation in pentane at 25 °C. Then, the powder was washed four times with dry pentane in order to remove the excess of complex affording V(=O)(O*t*Bu)$_3$/$SiO_{2\text{-}200}$ **(2)** as a colorless material. The reaction of [V(=O)(O*t*Bu)$_3$] proceeds with the consumption of almost all the surface free (or “isolated”) silanols of $SiO_{2\text{-}200}$, as shown from the irreversible disappearance of the $\nu_{O\text{-}H}$ stretching band at 3747 cm^{-1}

(Figure 1, Left). Importantly, the intensity of the other large $\nu_{O\text{-}H}$ band centered at 3600 cm^{-1}, attributed to vicinal silanols, did not decrease after reaction with the complex due to the low reactivity of these vicinal silanols. This phenomenon was already observed for the reaction of SiO_{2-200}, with several complexes of metal of groups IV, V and VI.[50] Concomitantly, two groups of bands appear in the 3200-2700 cm^{-1} and 1500-1300 cm^{-1} region, assigned respectively to ν(CH) and δ(CH) vibrations of the methyl groups of the perhydrocarbyl ligands.

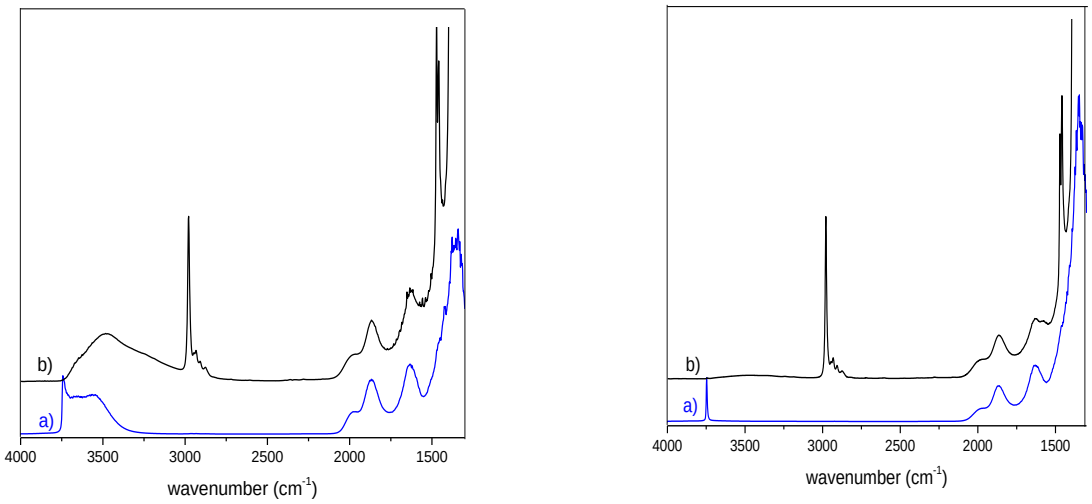

Figure 1. Left: IR-spectra of a) $SiO_{2\text{-}200}$ and b) after grafting of [V(=O)(O*t*Bu)$_3$] on $SiO_{2\text{-}200}$ **(2),** and **Right:** IR-spectra of a) $SiO_{2\text{-}700}$ and b) after grafting of [V(=O)(O*t*Bu)$_3$] on $SiO_{2\text{-}700}$ **(3)**

The amounts of vanadium and carbon, as quantified by elemental analysis of V(=O)(O*t*Bu)$_3$/SiO_{2-200} material, **(2)**, are 1.6 wt% V and 1.5 wt % C, which accounts for an atomic ratio of ca. 4.0 C/V. The vanadium loading of the material is thus 0.315 mmol.g^{-1} and since the concentration of silanols is ca. 0.86 mmol OH/g on SiO_{2-200},[40] this gives a V/OH ratio of 0.365. The quantification of the *t*BuOH evolved during the grafting reaction, was carried out by GC analysis, using octane as an internal standard. It leads to a release of 1.8 *t*BuOH/V. Thus, the results of these characterizations are in line with the formation of a major bipodal species bearing one tert-butoxide ligand, [(≡SiO)$_2$V(=O)(O*t*Bu)]. Further spectroscopic characterizations provided additional information on the grafting of [V(=O)(O*t*Bu)$_3$] on $SiO_{2\text{-}200}$. ^{1}H MAS NMR shows one signal at 1.4 ppm assigned to C**H**$_3$ protons (Figure S3) and one signal in ^{13}C CP MAS NMR at 28 ppm attributed to the carbon of the methyl groups (Figure 2). The lack of a significant signal for the quaternary carbon of the tert-butoxide ligand is most probably due to the larger chemical shift anisotropy, owing to a lower mobility of the surface species compared to the case of $SiO_{2\text{-}700}$ support (material **(3)**), as previously observed.[51,52] No improvement for the ^{13}C signal of the quaternary carbon was shown under the ^{13}C{^{1}H} MAS mode.

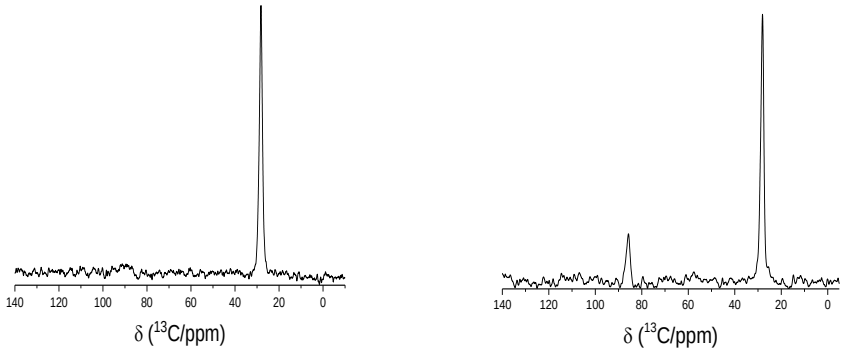

Figure 2. ^{13}CP CP MAS NMR of **Left:** V(=O)(O*t*Bu)$_3$/SiO$_{2\text{-}200}$ and **Right**: V(=O)(O*t*Bu)$_3$/SiO$_{2\text{-}700}$ (11.8 T, 10 kHz, $d_{1=}$ 5 s)

^{51}V NMR is a powerful technique that brings additional information on the coordination sphere and geometry of the vanadium centers in supported catalysts.[53,54] The ^{51}V MAS NMR of **(2)** reveals a signal with an isotropic chemical shift of -693 ppm (Figure 3, top), which represents an upfield shift of 51 ppm in comparison to [V(=O)(O*t*Bu)$_3$] molecular complex, **(1),** which shows a signal at -642 ppm (Figure S2). This result is consistent with the formation of a bipodal surface species on silica-$_{200}$. In fact, the upfield shift was also reported in literature, for a [V(=O)(O*i*Pr)$_3$] complex with a ^{51}V NMR signal at -630 ppm, that shifts to -650 ppm when two O*i*Pr ligands of this complex are exchanged by two siloxy groups from the silica surface, leading to [(≡SiO)$_2$V(=O)(O*i*Pr)] supported species.[55]

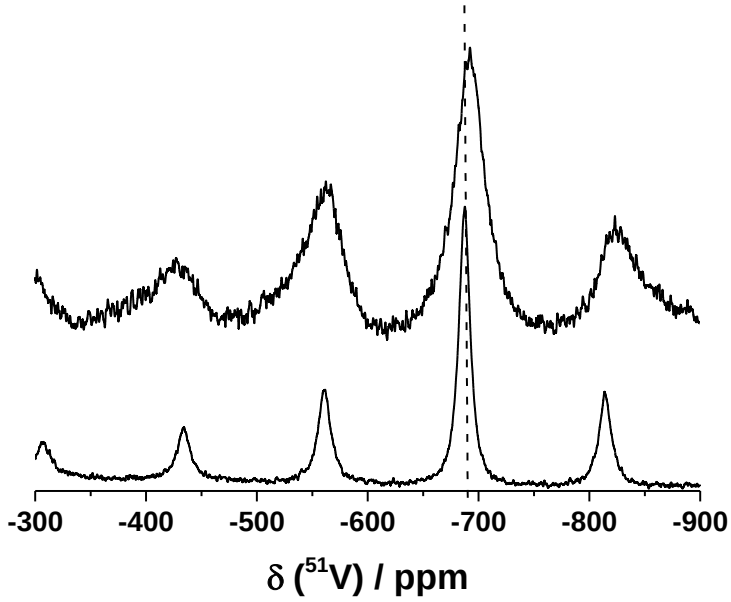

Figure 3. ^{51}V MAS NMR spectra of: V(=O)(O*t*Bu)$_3$/SiO$_{2\text{-}200}$, **(2)** (top) (7.1 T, 10 kHz, d_1= 1 s) and V(=O)(O*t*Bu)$_3$/SiO$_{2\text{-}700}$, **(3)** (down) (7.1 T, 10 kHz, d_1= 1 s)

The UV-Vis spectrum of **(2)**, comprises absorption bands starting from 200-400 nm (Figure 4). The absence in the spectrum of any absorption in the d → d transition part, suggests that the supported vanadium is in its highest oxidation state.[56] The broad peak in the UV region (λmax = 267 nm) can be assigned to a ligand to metal charge transfer (LMCT) originated from the tert-butoxide ligands. The energy edge (E_g) derived from the O→V charge transfer peak (determined from the intercept of the $[F(R_\infty)h\nu]^2$ vs $h\nu$ plot in the low energy rise) reflects the degree of vanadia polymerization.[57] This value is extrapolated to be 3.58 eV for **(2)**, suggesting that the vanadium sites are present as monomer on the surface.[58]

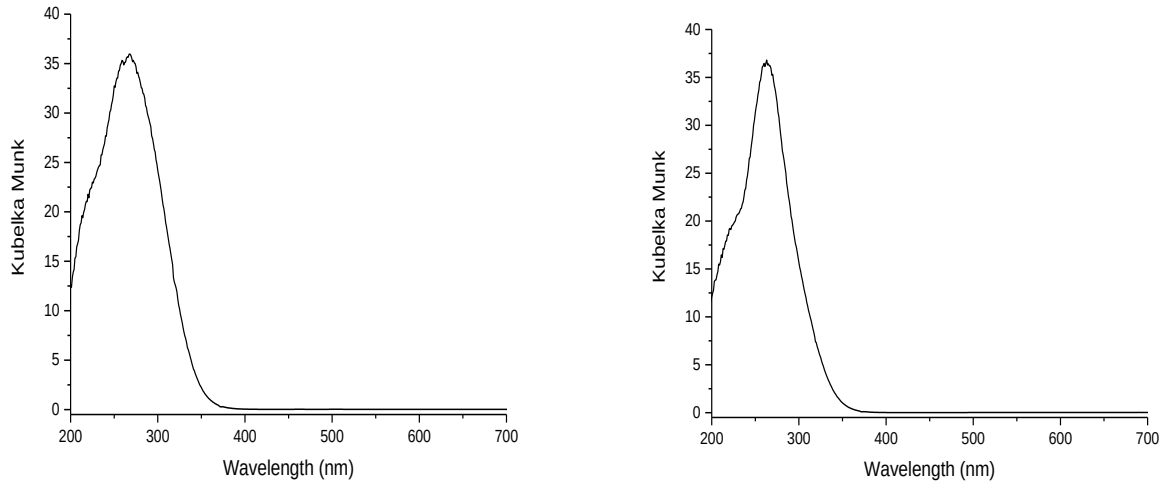

Figure 4. UV-Vis spectrum of **(2)** (left) and **(3) (**right)

XANES analysis of the molecular complex on $SiO_{2\text{-}200}$.

Additional information on the vanadium coordination geometry, its structural environment and oxidation state in the case of the molecular complex, **(1),** and materials **(2)** and **(3)** were given by X-ray absorption spectroscopy. Normalized V K-edge XANES spectra of the molecular complex, [V(=O)(O*t*Bu)$_3$], of the presumed [(≡SiO)$_2$V(=O)(O*t*Bu)] complex in material **(2)**, obtained from the grafting of [V(=O)(O*t*Bu)$_3$] onto $SiO_{2\text{-}200}$ are shown in Figure 5. In the two spectra (a and b), there is a prominent pre-edge peak. This pre-edge feature arises from electronic transitions from 1s core levels to the empty 3d levels, more or less 4p hybridized by the ligands of vanadium. These electronic transitions become electric-dipolar allowed in the absence of an inversion center. In this case, the loss of symmetry allows partial overlapping and mixing of the unfilled d states of the metal with its 4p orbitals. Several studies of the V K-edge XANES features have considered the pre-edge intensity as well as its absolute position to determine both the vanadium oxidation state and its symmetry.[59–61] The position of the pre-edge peak on its own is generally insufficient to evaluate accurately the vanadium oxidation state.

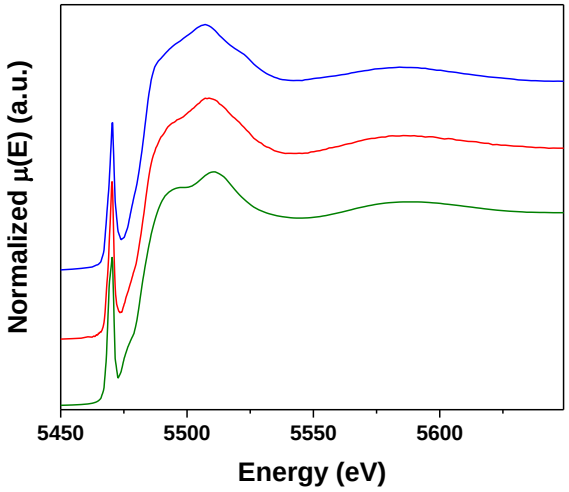

Figure 5. XANES: of (a) [V(=O)(O*t*Bu)$_3$] molecular complex, **(1)**; (b) V(=O)(O*t*Bu)$_3$/SiO$_{2\text{-}200}$ **(2)**; (c) V(=O)(O*t*Bu)$_3$/SiO$_{2\text{-}200}$ heated at 500°C **(2a)**.

The position and intensity of the main pre-edge peak along with the position of the edge of different vanadium compounds studied are reported in Table 1. For the molecular complex, **(1)** and material **(2)** referenced above, the position of the pre-edge peak at ca. 5470.4 eV and its high intensity (0.79 to 0.85) are consistent with those observed in other complexes or materials containing $V^{(V)}$ in a tetrahedral symmetry.[60] Moreover, the position of the K-edge of the three samples, shifted by 16 to more than 18 eV to higher energy relative to the metal foil, are within the range of K-edge energies reported for known $V^{(V)}$ compounds.[59]

Table 1. Positions and intensities of the pre-edge signal and edge positions in the V K-edge XANES of several vanadium samples.

Sample	Pre-edge signal position[a] (eV)	Pre-edge signal intensity[b] (a.u.)	Edge position[a,c] (eV)
$V^{(0)}$ (metal foil)			5465.1
[V^{III}(Mes)$_3$·THF]	5466.6	0.55	5474.2
[V^{IV}(=O)SO$_4$(H$_2$O)$_x$]	5469.8	0.48	5476.5
[V^{V}(=O)(O*t*Bu)$_3$] **(1)**	5470.4	0.79	5481.9
V(O)(O*t*Bu)$_3$/SiO$_{2\text{-}200}$ **(2)**	5470.3	0.85	5483.4
V(=O)(O*t*Bu)$_3$ /SiO$_{2\text{-}200}$ heated at 500°C **(2a)**	5470.5	0.81	5483.5
V(=O)(O*t*Bu)$_3$ /SiO$_{2\text{-}700}$ **(3)**	5470.3	0.85	5483.2
V(=O)(O*t*Bu)$_3$ /SiO$_{2\text{-}700}$ heated at 500°C **(3a)**	5470.4	0.81	5483.6

[a] Relative to a calibration with a vanadium foil (5465.1 eV); A ± 0.3 eV error is estimated on the energy. [b] Intensity normalized to the step height of the K-edge. [c] Defined as the first inflexion point after the pre-edge peak.

Reactivity of [V(=O)(O*t*Bu)$_3$] with a silica dehydroxylated at 700 °C, material (3) synthesis

The same amorphous silica support was partially dehydroxylated at 700 °C ($SiO_{2\text{-}700}$) under high vacuum (10^{-5} mbar) in order to compare the structure of the supported species on the resulting material, **(3)**, to those obtained on material **(2)**, after the grafting of [V(=O)(O*t*Bu)$_3$] on $SiO_{2\text{-}200}$. $SiO_{2\text{-}700}$ presents a density of ca. 0.70 OH per nm^2 corresponding to 0.27 mmol OH.g^{-1}.[39] The impregnation of [V(=O)(O*t*Bu)$_3$] on $SiO_{2\text{-}700}$ in a pentane solution occurred at room temperature for 4h. After an intensive washing with pentane to remove the excess of the complex and a drying under high vacuum, a white powder was obtained **(3)**. The infrared spectroscopy of V(=O)(O*t*Bu)$_3$/$SiO_{2\text{-}700}$ **(3)** revealed the consumption of all the isolated silanols initially present on $SiO_{2\text{-}(700)}$, shown by the disappearance of the $\nu_{O\text{-}H}$ band at 3747 cm^{-1} (Figure 1, Right). Simultaneously, alkyl bands in the range of 3000-2800 cm^{-1} ($\nu_{C\text{-}H}$) and 1500-1300 cm^{-1} (δ_{CH_2} and δ_{CH_3}) appeared, confirming the grafting of the vanadium complex on the silica surface. Elemental analysis of material **(3)** indicates V and C wt% contents of 1.12 and 2.23 wt%, respectively, corresponding to an atomic ratio of 7.9 C/V. The V/OH ratio is ca. 0.815, since 0.220 mmol of V/g of silica are grafted on the surface. GC analysis of *t*BuOH released during the grafting revealed a release of 0.88 *t*BuOH/V after reaction. The comparison of the mass balance analyses obtained after the grafting of [V(=O)(O*t*Bu)$_3$] on $SiO_{2\text{-}200}$ and $SiO_{2\text{-}700}$ are resumed in Table 2. It is obvious from these results that the structure of the resulting species in materials **(2)** and **(3)** depends on the dehydroxylation temperature of the support. Thus, the characterization results suggest the formation of a major monopodal species, [(≡SiO)V(=O)(O*t*Bu)$_2$] for **(3)**, from $SiO_{2\text{-}700}$, and a bipodal species [(≡SiO)$_2$V(=O)(O*t*Bu)] for **(2)**, from $SiO_{2\text{-}200}$.

Table 2. Mass balance analysis for the grafting of [V(=O)(O*t*Bu)$_3$], **(1)**, onto silica.

Supports	$\%_{wt}$ V[c]	$\%_{wt}$ C[d]	C/V ratio	*t*BuOH/V
$SiO_{2\text{-}200}$	1.6	1.5	4	1.8
$SiO_{2\text{-}700}$	1.12	2.23	7.9	0.88

[c]The error on V is < 5 %.[d] The error on the C elemental analyses is ±1 a.m.u.

The characterization of material **(3)** by ^{1}H MAS NMR shows a similar result to the one observed for material **(2)**. The spectrum also consists in a main signal at 1.4 ppm corresponding to C**H$_3$** protons of tert-butoxide ligands (Figure S3). The ^{13}C CP MAS spectrum of V(=O)(O*t*Bu)$_3$/$SiO_{2\text{-}700}$, **(3)**, shows two signals at 86 ppm and 28 ppm, assigned to quaternary carbon and **C**H$_3$ terminal groups, respectively (Figure 2, Right). It is important to note that the signal attributed for the quaternary carbon

at 86 ppm is visible compared to **(2)**. This is either due to the presence of two tert-butoxide ligands on the surface (higher concentration), compared to the main surface complex of **(2)**, or to a higher mobility of the surface species in **(3)**, leading to a narrower chemical anisotropy. A signal centered at -687 ppm appears in the ^{51}V MAS NMR spectrum, attributed to the monopodal complex [(≡SiO)V(=O)(O*t*Bu)$_2$] (Figure 3, down). This chemical shift corresponds to an up-field shift of -45 ppm compared to the precursor [V(=O)(O*t*Bu)$_3$] (-642 ppm). Nevertheless, the observed chemical shift is rather similar to the bipodal [(≡SiO)$_2$V(=O)(O*t*Bu)] (-693 ppm).[42,55] Taking into consideration the peak broadening (FWHM ≈ 35 ppm), the podality of supported [V(=O)(O*t*Bu)$_3$] is indistinguishable by ^{51}V MAS NMR spectroscopy. The UV-vis spectrum of [(≡SiO)V(=O)(O*t*Bu)$_2$] consists in an absorption band between 200 and 400 nm with a λ_{max} = 262 nm, corresponding to ligand to metal charge transfer (LMCT $O^{2-} \rightarrow V^{5+}$) (Figure 4). Similarly to the bipodal species, no absorption band at 650 nm was observed, hence, the vanadium adsorbed on the surface has the highest oxidation state (+V).[56] The energy edge (Eg) is 3.6 eV (compared to 3.58 eV in the case of V(=O)(O*t*Bu)$_3$/SiO$_{2\text{-}200}$), which is in line with the formation of monomers vanadium sites on the surface.[58]

XANES analysis of the molecular complex on SiO$_{2\text{-}700}$.

The normalized V K-edge XANES spectra of the molecular complex, [V(=O)(O*t*Bu)$_3$], of [(≡SiO)V(=O)(O*t*Bu)$_2$] complex, obtained from the grafting of [V(=O)(O*t*Bu)$_3$] onto SiO$_{2\text{-}700}$ are shown in Figure 6. The position and intensity of the main pre-edge peak along with the position of the edge of these vanadium compounds are also reported in Table 1. For V(=O)(O*t*Bu)$_3$/SiO$_{2\text{-}700}$ supported species, the position of the pre-edge peak (5470.3 eV), its relative intensity (0.85) and the position of the edge (5483.2 eV) are also indicative of V(V) tetrahedral species.

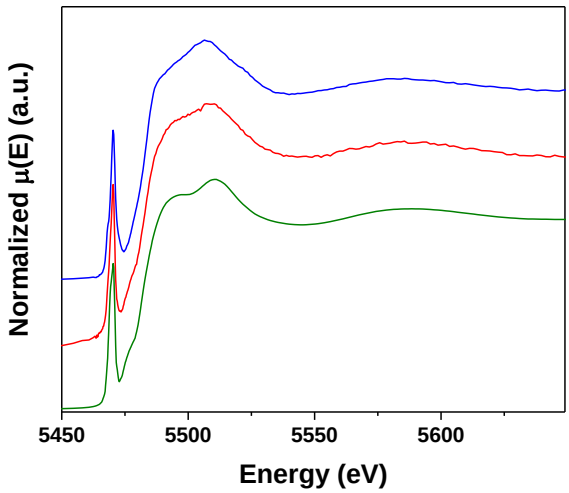

Figure 6. XANES of (a) [V(=O)(O*t*Bu)$_3$] molecular complex (**1**); (b) V(=O)(O*t*Bu)$_3$/SiO$_{2\text{-}700}$, **(3)**; (c) V(=O)(O*t*Bu)$_3$/SiO$_{2\text{-}700}$ heated at 500°C, **(3a)**.

In conclusion, well-defined single site catalysts with low loading of vanadium were obtained by grafting [V(=O)(O*t*Bu)$_3$] onto $SiO_{2\text{-}200}$ and $SiO_{2\text{-}700}$. A bipodal as major species was formed on $SiO_{2\text{-}200}$ surface noted as [(≡SiO)$_2$V(=O)(O*t*Bu)] **(2)**. The grafting of [V(=O)(O*t*Bu)$_3$] on $SiO_{2\text{-}700}$ led to monopodal species represented by [(≡SiO)V(=O)(O*t*Bu)$_2$] **(3)** (Scheme 2).

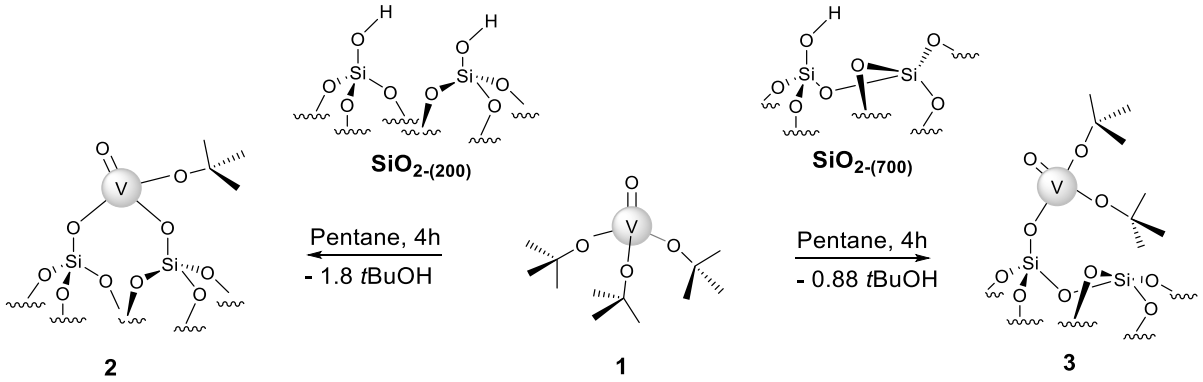

Scheme 2. Grafting of [V(=O)(O*t*Bu)$_3$] on $SiO_{2\text{-}200}$ and $SiO_{2\text{-}700}$ leading to structurally distinct surface species

Tripodal species

Controlled thermolyses of [(≡SiO)V(=O)(O*t*Bu)$_2$], **(2)** from 25 to 300 °C (for 2 h), 400 °C (for 2 h) as well as 500 °C (for 2 h) were conducted under vacuum in a reactor equipped with a cold trap (liquid N_2) in order to collect the gas phase evolved during the process. The analysis of the gas phase by GC after thermal treatment at 300 °C revealed the formation 0.88 isobutene/V for **(2)**, and some traces of *t*BuOH were observed. As reported in the case of silica supported Mo and W complexes bearing oxo tert-butoxide ligands,[46,47] the formation of isobutene is triggered by the elimination from a methyl group of a H in β-position of the oxygen coordinated to the metal, M-**O**-C(Me)$_2$-CH$_2$-**H**, to form a hydroxy intermediate, M-OH. This step can be assisted by the presence of an oxo ligand in the coordination sphere of vanadium.

The DRIFT analysis of the resulting materials from bipodal [(≡SiO)$_2$V(=O)(O*t*Bu)] species after heating at 300 °C revealed the total disappearance of the alkyl vibrational bands in the range of 3000−2800 cm^{-1} and 1500-1300 cm^{-1}, assigned respectively to ν(CH), δ(CH) vibrations from the perhydrocarbyl ligands (Figure 7, Left). At 300 °C (after 2h), we observed the reappearance of isolated silanol groups at 3747 cm^{-1} as well as the appearance of a new band at 3660 cm^{-1} attributed to $\nu_{VO\text{-}H}$.[62,63] At 400 °C, the intensity of the band characteristic of $\nu_{SiO\text{-}H}$ increases while the one of $\nu_{VO\text{-}H}$ band decreases. At 500 °C, we observed the absence of the vibration band attributed to VO-H elongation vibration, accompanied by the decrease in intensity of the ≡SiO-H silanols vibration band. This phenomenon could be explained by a partial condensation of V-OH with the remaining silanols, leading to the formation of water and V-OSi bonds and thus tripodal V oxo surface species (Scheme S1).

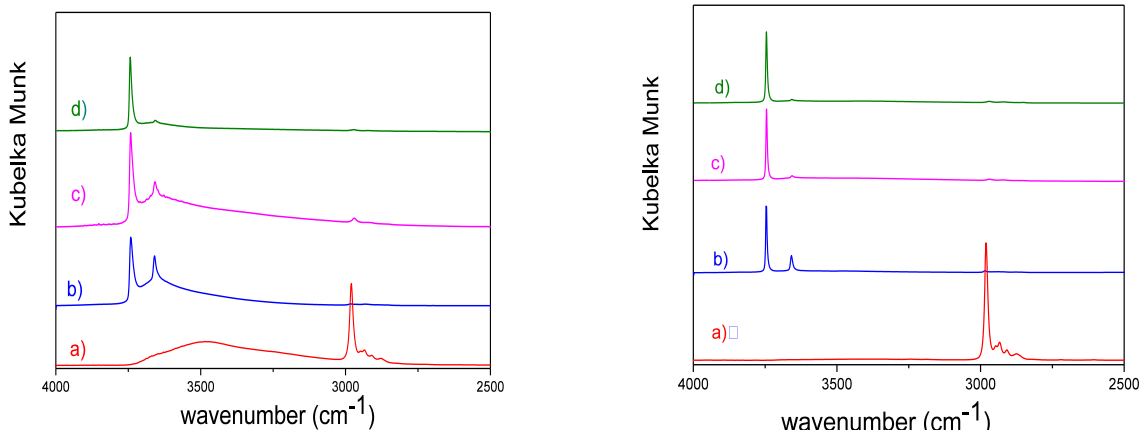

Figure 7. Left. IR-spectra of **a)** V(=O)(O*t*Bu)$_3$/SiO$_{2\text{-}200}$ **(2)**, and then thermally treated at: **b)** 300 °C, **c)** 400 °C, and **d)** 500 °C; **Right**. IR-spectra of **a)** V(=O)(O*t*Bu)$_3$/SiO$_{2\text{-}700}$ **(3)**, and then thermally treated at: **b)** 300 °C, **c)** 400 °C and **d)** 500 °C

Similarly, these phenomena were also observed by ^{1}H MAS NMR of **(2)** thermally treated from 25 to 500 °C (Figure 8, Left). The intense signal at 1.3 ppm attributed to the methyl groups of tert-butoxide ligands decreased, and almost disappeared at 300 °C. Simultaneously, a signal at 1.8 ppm corresponding to isolated silanol groups appears at 300 °C and increases during the thermolysis (up to 500 °C). The release of isobutene during the thermolysis reaction and the appearance of silanol groups along with the disappearance of vanadium hydroxy intermediates, suggests that supported surface species in **(2)**, lead to the formation of the targeted tripodal oxo species [(≡SiO)$_3$V(=O)] **(2a)** upon a thermal treatment under vacuum.

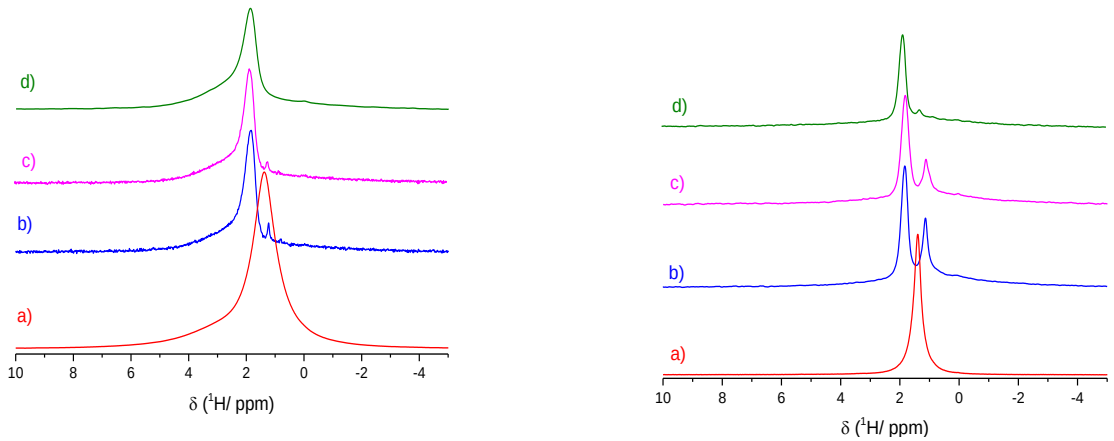

Figure 8. Left. ^{1}H NMR spectra of **a)** V(=O)(O*t*Bu)$_3$/SiO$_{2\text{-}200}$ **(2),** and then thermally treated at: **b)** 300 °C, **c)** 400 °C, and **d)** 500 °C; **Right**. ^{1}H NMR spectra of **a)** V(=O)(O*t*Bu)$_3$/SiO$_{2\text{-}700}$ **(3),** and then thermally treated at: **b)** 300 °C, **c)** 400 °C and **d)** 500 °C

The same procedure including a thermal treatment under vacuum at progressively increasing temperatures, has been applied to surface species of **(3)**. This leads to similar observations from DRIFT and ^{1}H MAS NMR data (right parts of Figure 7 and Figure 8, respectively), allowing to the formation of a tripodal vanadium oxo on $SiO_{2\text{-}700}$ **(3a)** with a release of 1.9 isobutene/V. The resulting vanadium surface species **(2a)** and **(3a)** were further characterized by XANES, UV-vis and ^{51}V MAS NMR.

XANES of the tripodal species

Both tripodal vanadium systems obtained on silica were characterized by XANES spectroscopy to provide additional details on the vanadium structural environment after thermal treatment of the grafted species. Normalized V K-edge XANES spectra of tripodal systems on $SiO_{2\text{-}200}$ **(2a)** and $SiO_{2\text{-}700}$ **(3a)**, in contrast with [V(=O)(O*t*Bu)$_3$] and species **(2)** and **(3)** are shown in Figure 5,c and Figure 6,c. The position and intensity of the main pre-edge peak along with the position of the edge of targeted species [(≡SiO)$_3$V(=O)] is compared to molecular complex [V(=O)(O*t*Bu)$_3$], surface species **(2)** [(≡SiO)$_2$V(=O)(O*t*Bu)] and **(3)** [(≡SiO)V(=O)(O*t*Bu)$_2$] (Table 1). Similar to the complex and to the grafted species, the XANES spectra of tripodal oxo species **(2a)** and **(3a)** displayed a pre-edge peak located at ca. 5470.4 eV. The relative intensities of these pre-edges are high and range from 0.85 (for grafted species **(2)** and **(3)**) to 0.81 for tripodal species **(2a)** and **(3a)**. These results are consistent with those observed for other complexes or materials containing V(V) in a tetrahedral symmetry.[60] Moreover, the position of the K-edge of the samples, shifted from 16 to more than 18 eV to higher energy relative to the metal foil, are within the range of K-edge energies reported for known V(V) compounds.[59]

Additional characterizations of the surface tripodal oxo species **(2a)** and **(3a)** were given by UV-vis spectroscopy (Figure 9). This method allows the detection of isolated V(IV), V(V) and vanadium oligomeric species. The UV-vis spectra of **(2a)**, [(≡SiO)$_3$V(=O)] species on $SiO_{2\text{-}200}$ exhibited a band at 253 nm along with a shoulder at 286 nm attributed to $\pi(t2)\rightarrow d(e)$ and $\pi(t1)\rightarrow d(e)$ oxygen-to-tetrahedral V(V) charge transfer transitions, involving oxygen in bridging (V-O-Si) and terminal (V=O) positions, respectively, in agreement with reported literature.[64] A similar result was obtained in the UV-vis spectrum of **(3a)**, [(≡SiO)$_3$V(=O)] on $SiO_{2\text{-}700}$ with two bands at 256 and 287 nm. The absence of (d-d) transitions in the 600-800 nm range indicates that V(IV) species are not significantly present. Indeed, the energy edge (Eg) of the tripodal V species on $SiO_{2\text{-}200}$ and $SiO_{2\text{-}700}$ are ca. 3.50 and 3.35 eV, respectively (compared to 3.58 and 3.6 eV in the case of **(2)**, V(=O)(O*t*Bu)$_3$/$SiO_{2\text{-}200}$ and **(3)**, V(=O)(O*t*Bu)$_3$/$SiO_{2\text{-}700}$, respectively). The slight red-shift in the energy edge when transforming the grafted complexes into the tripodal species may be due to the creation of supplementary restrains

around the deformed tetrahedral vanadium centers. These results are in agreement with the formation of monomeric vanadium sites on the surface, as supported by XANES and ^{51}V MAS NMR.

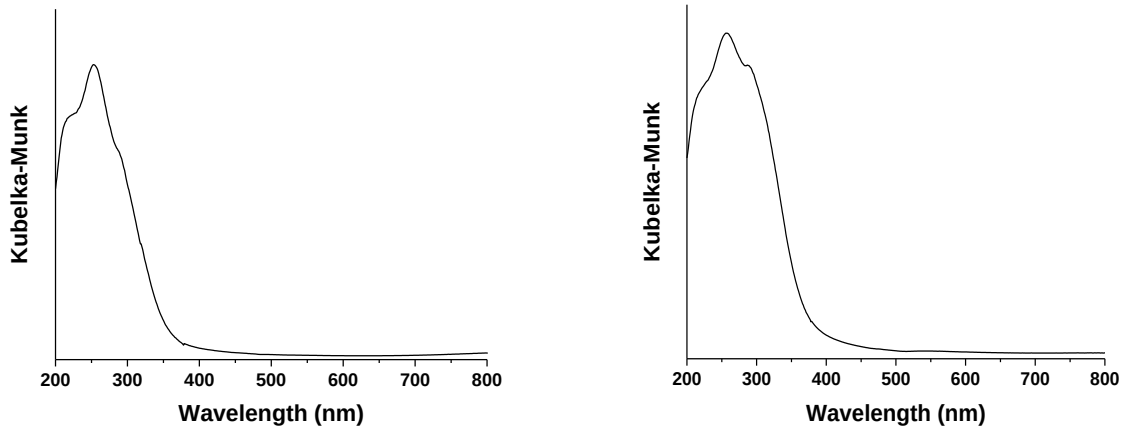

Figure 9. UV-vis of **Left: (2a)** and **Right: (3a)**

^{51}V MAS NMR is a complementary technique to IR, ^{1}H MAS NMR, XANES and UV-vis used to identify the surface vanadia species on the supported catalysts. Due to the importance in catalysis of the isolated tetrahedral vanadium complexes on various supports, the intensive ^{51}V solid-state NMR characterization of these types of catalysts by several groups showed that the chemical shift is generally in the range of -460 to -700 ppm.[53,65–67] The attribution of the signals in the ^{51}V NMR spectrum of these materials remains challenging due to the lack of supporting models (such as $(Ph_3SiO)_3V(=O)$ and vanadium oxo containing POMSS)[68,69] and to the variety of experimental conditions during the NMR acquisition.[70,71] Grant et al.[72] have studied by ^{51}V MAS NMR silica-supported vanadia catalysts prepared by impregnation with a surface coverage between 1.3 to 15.4 $V{\cdot}nm^{-2}$. In the ^{51}V NMR spectra obtained, the authors observed two different isotropic shifts, depending on the surface coverage of vanadium. For the materials prepared with the highest vanadium content (13.4 and 15.4 $V{\cdot}nm^{-2}$), a sharp peak appeared at -614 ppm, corresponding to the distorted trigonal bipyramidal geometry of crystalline V_2O_5, which is in line with previous work revealing close isotropic shift of crystalline V_2O_5 at −612 ppm[73] or −610 ppm.[53] In parallel, another signal was also observed at -675 ppm in all samples, but its intensity in the case of catalysts prepared with lower coverage of vanadium, in particular for 1.3 $V{\cdot}nm^{-2}$, was very low. This signal is attributed to dispersed monomeric species, $[(\equiv SiO)_3V(=O)]$.[74] Recently, Jaegers. et al.,[70] confirmed these MAS NMR attributions, by employing faster spinning rates (above 30 kHz) at a higher field (19.975 T), and reported a better resolution of the signal assigned to tripodal V species (at -675 ppm), even at low V content (0.6 $V.nm^{-2}$). In the case of the supported species of **(2a)** and **(3a),** with low V coverages, ca. 1.1 and 0.8 $V.nm^{-2}$, respectively, ^{51}V MAS NMR

revealed a similar signal with a chemical shift of -670 ppm for both samples (Figure 10), attributed to [(≡SiO)$_3$V(=O)] isolated vanadium surface species, on $SiO_{2\text{-}200}$ and $SiO_{2\text{-}700}$ (Scheme 3).

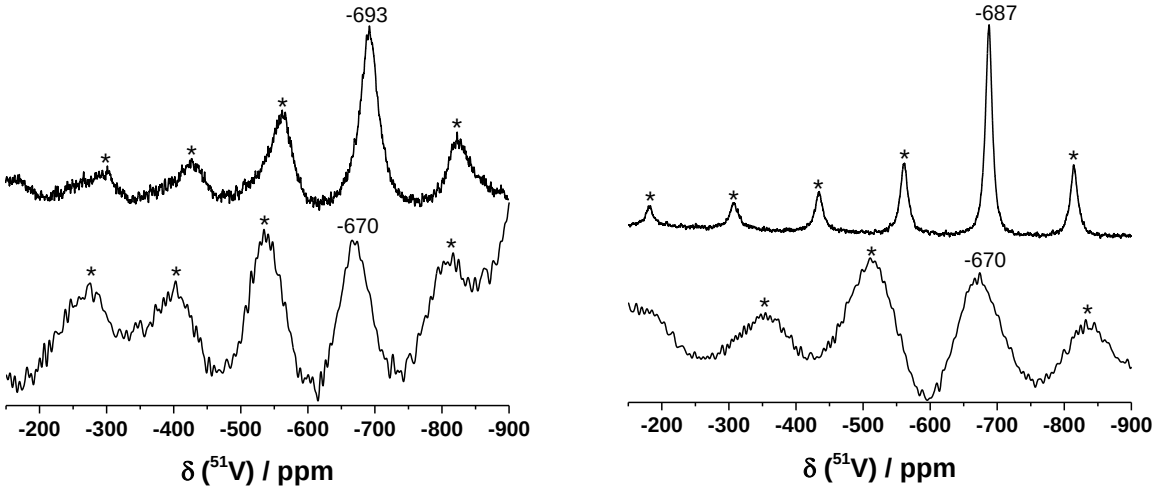

Figure 10. Solid-state ^{51}V NMR spectra of: **Left:** V(=O)(O*t*Bu)$_3$/$SiO_{2\text{-}200}$ **(2)** (7.1 T, 10 kHz, d_1= 1 s) (top) and [(≡SiO)$_3$V(=O)] **(2a)** (down) (7.1 T, 10 kHz, d_1= 1 s), and **Right:** V(=O)(O*t*Bu)$_3$/$SiO_{2\text{-}700}$ **(3)** (7.1 T, 10 kHz, d_1= 1 s) (top) and [(≡SiO)$_3$V(=O)] **(3a)** (down) (7.1 T, 12 kHz, d_1= 1 s). Grafted species in **(2)** and **(3)** revealed a major peak at -693 and -687 ppm respectively. Tripodal species in **(2a)** and **(3a)** exhibited a major peak at -670 ppm.

The above characterization by DRIFT, ^{1}H and ^{51}V MAS NMR, XANES, mass balance analysis, UV-vis of the resulting species after a thermal treatment of bipodal (**2**) and monopodal (**3**) vanadium species, revealed the formation of tripodal vanadium species, [(≡SiO)$_3$V(=O)] in **(2a)** and **(3a)** materials.

The mechanism of the formation of these active species would be similar on $SiO_{2\text{-}200}$ and $SiO_{2\text{-}700}$. It has been proposed that a hydrogen transfer from a methyl group of a *tert*-butoxy ligand to the vanadyl oxygen occurs, leading to a V-OH fragment. The latter reacts with a siloxane bridge from the support by a Si-O-Si ring opening, leading to the formation of new isolated silanols as described in Scheme 3 (e.g on $SiO_{2\text{-}200}$). The hydrogen transfer to the vanadyl oxygen can occur either by a transfer of one hydrogen to the oxo ligand, or by direct migration of one hydrogen from a methyl group to the oxygen of a tert-butoxide ligand, thus releasing a *t*BuOH molecule. It was indeed demonstrated that the thermal treatment of metal derivatives of -OSi(O*t*Bu)$_3$ led to the direct elimination of isobutylene, even at low temperatures (100 - 150 °C) to form silanols without any assistance of other ligands.[75]

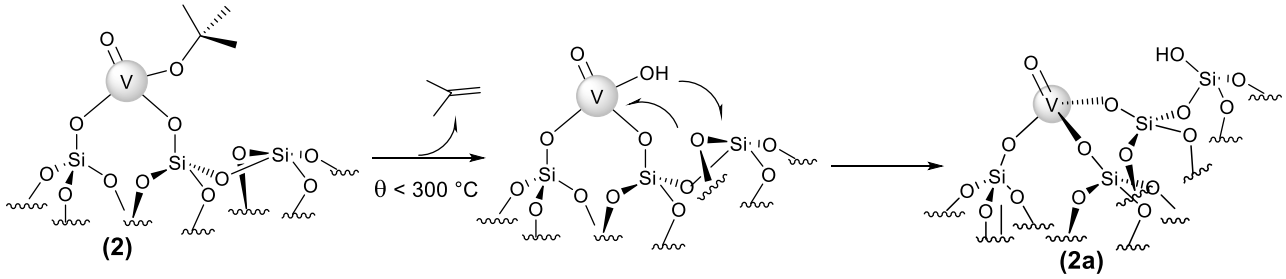

Scheme 3. Proposed mechanism for the formation of [(≡SiO)$_3$V(=O)] species

Catalytic properties

The catalytic behavior of the tripodal V species supported on $SiO_{2\text{-}200}$ and $SiO_{2\text{-}700}$ was evaluated in the non-oxidative dehydrogenation of propane. A continuous fixed-bed type reactor was used, under the following operating conditions: θ = 540 °C, P = 1 bar and a total flow of 5 mL.min^{-1} (20 % of C_3H_8 in Ar). The reactor was heated from room temperature to 540 °C under a flow of 4 mL.min^{-1} of argon and then propane was introduced at 540 °C.

When propane was fed to the catalytic bed of tripodal V obtained on $SiO_{2\text{-}200}$ **(2a)**, a conversion of 19 % was reached at early times on stream and slightly decreased to 17 % after 1000 min (Figure 11). At that time, the selectivity toward propene was 84.5 %, and the by-products included methane (6.8 %), ethene (4.7 %) and ethane (2.5 %) as well as traces of C4 (< 2%) (Figure 12, Left). On the other hand, tripodal V on $SiO_{2\text{-}700}$ **(3a)** exhibited a different behavior in function of time on stream. A lower initial conversion of 15% followed by a gradual deactivation was observed, leading to 10.4% after 1000 min. Initially, the products comprised propene (88.4%), methane (6.8%), ethane (2.4%) and ethane (2.4 %). However, after 1000 min, the selectivity toward methane increased to 11.4% and propene decreased to 81.7% while ethane and ethene slightly increased to 3.6% and 3.2%, respectively. The activity and selectivity observed with **(2a)**, composed of tripodal V species on $SiO_{2\text{-}200}$ seems better than those with **(3a)**, composed of tripodal V species on $SiO_{2\text{-}700.}$ Such tendency was previously obtained in the case of vanadium species resulting from the grafting of O=V(mesityl)$_3$ complex on $SiO_{2\text{-}200}$ and on $SiO_{2\text{-}700}$.[40] This is probably due to the difference in the local structure of the tripodal V on a silica pretreated at different temperature. This difference in terms of structure has been also observed in the ^{51}V solid-state NMR of the tripodal species [(≡SiO)$_3$V(=O)] obtained on $SiO_{2\text{-}200}$ and $SiO_{2\text{-}700}$ after a thermal treatment. In fact, the larger signal observed in the case of vanadium supported on $SiO_{2\text{-}700}$ **(3a)**, is attributed to the presence of different tetrahedral vanadium species, with the same coordination sphere but different local environment, which could explain the difference in terms of catalytic activity.

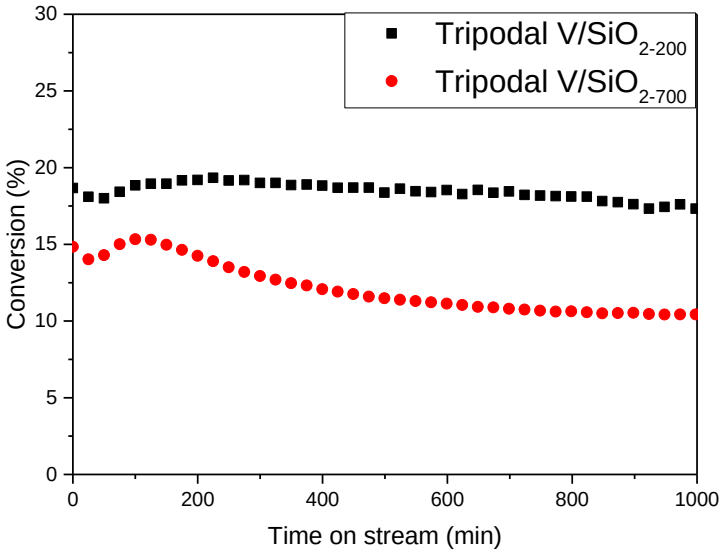

Figure 11. Propane conversion catalyzed by vanadium tripodal species supported on $SiO_{2\text{-}200}$, **(2a)** and on $SiO_{2\text{-}700}$, **(3a)**. Conditions: P= 1 bar; θ= 540 °C; Total flow = 5 mL.min^{-1} (20 % C_3H_8 in Ar)

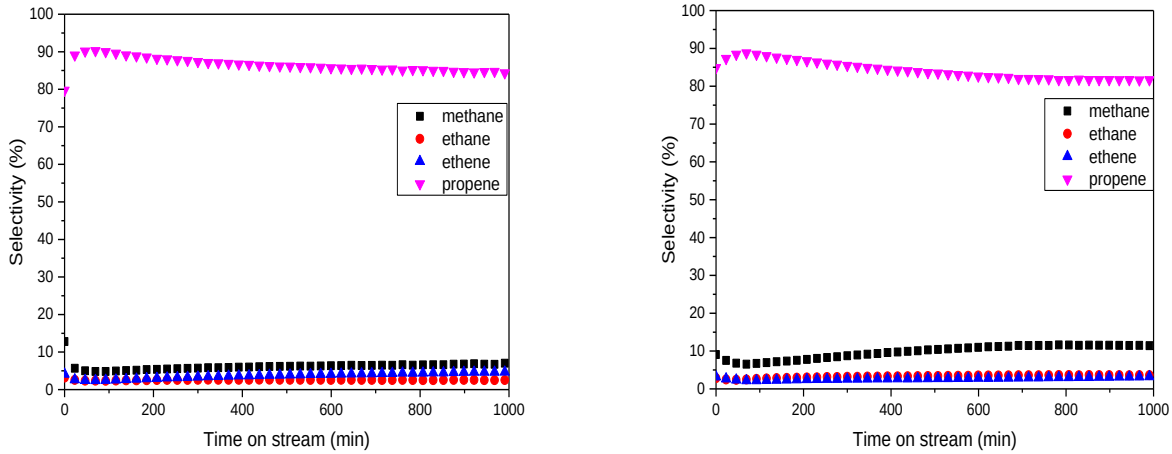

Figure 12. Selectivities obtained for propane conversion with vanadium tripodal species supported on $SiO_{2\text{-}200}$, **(2a)** (Left) and $SiO_{2\text{-}700}$, **(3a)** (Right). Conditions: P= 1 bar; θ= 540 °C; Total flow = 5 mL.min^{-1} (20 % C_3H_8 in Ar)

The present catalytic results can be directly associated to the vanadium tripodal species obtained through SOMC. These silica supported vanadium species exhibit different behavior in the propane dehydrogenation reaction with respect to conventional V_2O_5/SiO_2 catalysts prepared by aqueous impregnation.[13] This is potentially due to the presence of different vanadia species (from monomeric to oligomeric) on the surface of the latter catalyst. The determination of the mechanism and of the nature of the active species in each step is of high interest. However, these key-issues cannot be addressed with our current ex-situ characterization techniques. As reported for chromium, it is

reasonable to assume that the structure of the active species in PDH, is a tripodal $V^{(III)}$, [(≡SiO)$_3$V]. In fact, at the initiation step, the first hydrogen abstraction of propane occurs on V=O ligand of [(≡SiO)$_3$V(=O)], yielding an intermediate $V^{(V)}$ bearing an alkyl and a hydroxy ligand. This latter species would then undergo a β-H elimination of the V coordinated propyl ligand, leading to the formation of V hydrido hydroxyl species and the release of one propylene. The reductive elimination of the water from the V hydrido hydroxyl species, would then lead to the formation of the active species, [(≡SiO)$_3$V$^{(III)}$], during propane dehydrogenation (Scheme S2).

The full catalytic cycle can be described by two mechanistic pathways. Both involve an initialization of a V-O bond of [(≡SiO)$_3$V] by a C-H activation of propane, giving V-propyl species and an adjacent SiOH group. The next step is comprised by a β-H transfer to give a V-H and a coordinated propylene. Following a new activation of C-H of propane, the products (propylene and hydrogen) are released. The latter reaction scheme has previously been reported for supported metal hydride catalysts.[76,77] The second mechanistic pathway may involve cleavage and reconstruction of the V-H species with propylene coordinated, resulting in direct product release and regeneration of the tripodal species, as described for the chromium(III) system.[78] This mechanism has been earlier proposed in several reports. Firstly, Harlin *et al.* who observed that the reduced V_2O_5 based catalyst has an enhanced activity in non-oxidative dehydrogenation of *n*-butane and *i*-butane, suggested that the reduced states of vanadium ($V^{(IV)}$ or $V^{(III)}$) are more active.[79] Moreover, Chen *et al.* have revealed the presence of $V^{(III)}$ as a V_2O_3 phase by XRD after the dehydrogenation of ethylbenzene under nitrogen at 550 °C.[80] In addition, Takahara *et al.* have studied the hydrogen treatment of silica supported V_2O_5, and suggested that a cleavage of V-O bonds has occurred with the formation of V-O-H sites adjacent to the $V^{(IV)}/V^{(III)}$, possible hydrides.[13] Hence, the $V^{(IV)}/V^{(III)}$ species are most likely responsible for the dehydrogenation whereas VO-H acidic sites are believed to trigger the formation of carbonaceous deposit which increases with time on stream. Advanced operando techniques and theoretical calculations should offer additional insights on the reaction mechanism (Scheme S3).

Conclusion

In conclusion, supported oxovanadium(V) complexes were prepared by surface organometallic chemistry from the grafting of the molecular complex [V(=O)(O*t*Bu)$_3$], **(1)**, onto $SiO_{2\text{-}200}$ and $SiO_{2\text{-}700}$, leading to materials exhibiting bipodal species [(≡SiO)$_2$V(=O)(O*t*Bu)] on $SiO_{2\text{-}200}$ **(2)** and monopodal species [(≡SiO)V(=O)(O*t*Bu)$_2$] on $SiO_{2\text{-}700}$ **(3)**. They were fully characterized by elemental analysis, IR, UV-Vis, solid state NMR (^{1}H, ^{13}C, ^{51}V) and XANES. A new original method has been developed in this work for the preparation of supported tetrahedral vanadium oxo tripodal species [(≡SiO)$_3$V(=O)]

via a thermal treatment of the grafted species, triggering β-H transfer and isobutene release. In addition to the characterization of all these tripodal species by mass balance analysis, IR, UV-Vis, solid-state NMR (^{1}H) and XANES spectroscopy, the characterization by ^{51}V MAS NMR allowed the confirmation of the chemical isotropic shift of tripodal V at -670 ppm, which is in agreement with recently reported results. The catalytic behavior of the resulting tripodal species was evaluated in the direct dehydrogenation of propane to propene, exhibiting high activity and propene selectivity. Importantly, the presented catalytic results are exclusively originated from the isolated tripodal species. Regarding the gradual deactivation of the catalyst generally reported and attributed to the formation of carbonaceous species, this phenomenon was barely observed in our case compared to the conventional V_2O_5 supported on silica catalysts, which presents V-O-H acidic sites responsible for the coke formation.

Note

The authors declare no competing financial interests.

Supporting information

NMR spectra and proposed reaction schemes.

Acknowledgements

This work was carried out as a part of the BIZEOLCAT project, which has received funding from the European Union's Horizon 2020 research and innovation program under grant agreement No. 814671. In particular, J. A. is grateful for her PhD grant. AdM thanks Olivier Mathon and Kiril Lomachenko for their help during the recording of the X-ray absorption spectra at ESRF, on beam line BM23.

References

(1) Sattler, J. J. H. B.; Ruiz-Martinez, J.; Santillan-Jimenez, E.; Weckhuysen, B. M. Catalytic Dehydrogenation of Light Alkanes on Metals and Metal Oxides. *Chem. Rev.* **2014**, *114* (20), 10613–10653. https://doi.org/10.1021/cr5002436.

(2) Hu, Z.-P.; Yang, D.; Wang, Z.; Yuan, Z.-Y. State-of-the-Art Catalysts for Direct Dehydrogenation of Propane to Propylene. *Chin. J. Catal.* **2019**, *40* (9), 1233–1254. https://doi.org/10.1016/S1872-2067(19)63360-7.

(3) Akah, A.; Al-Ghrami, M. Maximizing Propylene Production via FCC Technology. *Appl. Petrochem. Res.* **2015**, *5* (4), 377–392. https://doi.org/10.1007/s13203-015-0104-3.

(4) Mazoyer, E.; Szeto, K. C.; Norsic, S.; Garron, A.; Basset, J.-M.; Nicholas, C. P.; Taoufik, M. Production of Propylene from 1-Butene on Highly Active "Bi-Functional Single Active Site"

Catalyst: Tungsten Carbene-Hydride Supported on Alumina. *ACS Catal.* **2011**, *1* (12), 1643–1646. https://doi.org/10.1021/cs2004054.

(5) Mazoyer, E.; Szeto, K. C.; Basset, J.-M.; Nicholas, C. P.; Taoufik, M. High Selectivity Production of Propylene from 2-Butene: Non-Degenerate Pathways to Convert Symmetric Olefins via Olefin Metathesis. *Chem. Commun.* **2012**, *48* (30), 3611–3613. https://doi.org/10.1039/C2CC30172E.

(6) Mazoyer, E.; Szeto, K. C.; Merle, N.; Norsic, S.; Boyron, O.; Basset, J.-M.; Taoufik, M.; Nicholas, C. P. Study of Ethylene/2-Butene Cross-Metathesis over W-H/Al2O3 for Propylene Production: Effect of the Temperature and Reactant Ratios on the Productivity and Deactivation. *J. Catal.* **2013,** 301, 1-7. https://doi.org/10.1016/j.jcat.2013.01.016.

(7) Svelle, S.; Olsbye, U.; Joensen, F.; Bjørgen, M. Conversion of Methanol to Alkenes over Medium- and Large-Pore Acidic Zeolites: Steric Manipulation of the Reaction Intermediates Governs the Ethene/Propene Product Selectivity. *J. Phys. Chem. C* **2007**, *111* (49), 17981–17984. https://doi.org/10.1021/jp077331j.

(8) Liu, X.; Wang, M.; Zhou, C.; Zhou, W.; Cheng, K.; Kang, J.; Zhang, Q.; Deng, W.; Wang, Y. Selective Transformation of Carbon Dioxide into Lower Olefins with a Bifunctional Catalyst Composed of ZnGa2O4 and SAPO-34. *Chem. Commun.* **2018**, *54* (2), 140–143. https://doi.org/10.1039/c7cc08642c.

(9) Pawelec, B.; Guil-Lopez, R.; Mota, N.; Fierro, J. L. G.; Navarro Yerga, R. M. Catalysts for the Conversion of CO2 to Low Molecular Weight Olefins-A Review. *Materials* **2021**, *14* (22), 6952. https://doi.org/10.3390/ma14226952.

(10) Nawaz, Z. Light Alkane Dehydrogenation to Light Olefin Technologies: A Comprehensive Review. *Rev. Chem. Eng.* **2015**, *31* (5), 413–436. https://doi.org/10.1515/revce-2015-0012.

(11) Fridman, V. Z.; Xing, R. Deactivation Studies of the CrOx/Al2O3 Dehydrogenation Catalysts under Cyclic Redox Conditions. *Ind. Eng. Chem. Res.* **2017**, *56* (28), 7937–7947. https://doi.org/10.1021/acs.iecr.7b01638.

(12) Chalupka, K.; Thomas, C.; Millot, Y.; Averseng, F.; Dzwigaj, S. Mononuclear Pseudo-Tetrahedral V Species of VSiBEA Zeolite as the Active Sites of the Selective Oxidative Dehydrogenation of Propane. *J. Catal.* **2013**, *305*, 46–55. https://doi.org/10.1016/j.jcat.2013.04.020.

(13) Takahara, I.; Saito, M.; Inaba, M.; Murata, K. Dehydrogenation of Propane over a Silica-Supported Vanadium Oxide Catalyst. *Catal. Lett.* **2005**, *102* (3), 201–205. https://doi.org/10.1007/s10562-005-5856-4.

(14) Rossetti, I.; Fabbrini, L.; Ballarini, N.; Oliva, C.; Cavani, F.; Cericola, A.; Bonelli, B.; Piumetti, M.; Garrone, E.; Dyrbeck, H.; Blekkan, E. A.; Forni, L. V–Al–O Catalysts Prepared by Flame Pyrolysis for the Oxidative Dehydrogenation of Propane to Propylene. *Catal. Today* **2009**, *141* (3), 271–281. https://doi.org/10.1016/j.cattod.2008.05.020.

(15) Cheng, L.; Ferguson, G. A.; Zygmunt, S. A.; Curtiss, L. A. Structure-Activity Relationships for Propane Oxidative Dehydrogenation by Anatase-Supported Vanadium Oxide Monomers and Dimers. *J. Catal.* **2013**, *302*, 31–36. https://doi.org/10.1016/j.jcat.2013.02.012.

(16) Karakoulia, S. A.; Triantafyllidis, K. S.; Tsilomelekis, G.; Boghosian, S.; Lemonidou, A. A. Propane Oxidative Dehydrogenation over Vanadia Catalysts Supported on Mesoporous Silicas with Varying Pore Structure and Size. *Catal. Today* **2009**, *141* (3), 245–253. https://doi.org/10.1016/j.cattod.2008.05.024.

(17) Routray, K.; Reddy, K. R. S. K.; Deo, G. Oxidative Dehydrogenation of Propane on V2O5/Al2O3 and V2O5/TiO2 Catalysts: Understanding the Effect of Support by Parameter Estimation. *Appl. Catal. Gen.* **2004**, *265* (1), 103–113. https://doi.org/10.1016/j.apcata.2004.01.006.

(18) Carrero, C. A.; Schloegl, R.; Wachs, I. E.; Schomaecker, R. Critical Literature Review of the Kinetics for the Oxidative Dehydrogenation of Propane over Well-Defined Supported Vanadium Oxide Catalysts. *ACS Catal.* **2014**, *4* (10), 3357–3380. https://doi.org/10.1021/cs5003417.

(19) Wegener, S. L.; Marks, T. J.; Stair, P. C. Design Strategies for the Molecular Level Synthesis of Supported Catalysts. *Acc. Chem. Res.* **2012**, *45* (2), 206–214. https://doi.org/10.1021/ar2001342.
(20) Wu, Y.-L.; Han, Z.-F.; Yan, X.; Lang, W.-Z.; Guo, Y.-J. Effective Synthesis of Vanadium-Doped Mesoporous Silica Nanospheres by Sol-Gel Method for Propane Dehydrogenation Reaction. *Microporous Mesoporous Mater.* **2022**, *330*, 111616. https://doi.org/10.1016/j.micromeso.2021.111616.
(21) Kaphan, D. M.; Ferrandon, M. S.; Langeslay, R. R.; Celik, G.; Wegener, E. C.; Liu, C.; Niklas, J.; Poluektov, O. G.; Delferro, M. Mechanistic Aspects of a Surface Organovanadium(III) Catalyst for Hydrocarbon Hydrogenation and Dehydrogenation. *ACS Catal.* **2019**, *9* (12), 11055–11066. https://doi.org/10.1021/acscatal.9b02800.
(22) Muylaert, I.; Voort, P. V. D. Supported Vanadium Oxide in Heterogeneous Catalysis: Elucidating the Structure–Activity Relationship with Spectroscopy. *Phys. Chem. Chem. Phys.* **2009**, *11* (16), 2826–2832. https://doi.org/10.1039/B819808J.
(23) Nielsen, U. G.; Topsøe, N.-Y.; Brorson, M.; Skibsted, J.; Jakobsen, H. J. The Complete 51V MAS NMR Spectrum of Surface Vanadia Nanoparticles on Anatase (TiO2): Vanadia Surface Structure of a DeNOx Catalyst. *J. Am. Chem. Soc.* **2004**, *126* (15), 4926–4933. https://doi.org/10.1021/ja030091a.
(24) Izumi, Y.; Kiyotaki, F.; Yoshitake, H.; Aika, K.; Sugihara, T.; Tatsumi, T.; Tanizawa, Y.; Shido, T.; Iwasawa, Y. Structure of Low Concentrations of Vanadium on TiO2 Determined by XANES and Ab Initio Calculations. *Chem. Commun.* **2002**, No. 20, 2402–2403. https://doi.org/10.1039/B207159B.
(25) Kozlowski, R.; Pettifer, R. F.; Thomas, J. M. X-Ray Absorption Fine Structure Investigation of Vanadium(V) Oxide-Titanium(IV) Oxide Catalysts. 2. The Vanadium Oxide Active Phase. *J. Phys. Chem.* **1983**, *87* (25), 5176–5181. https://doi.org/10.1021/j150643a023.
(26) Wolke, S. I.; Buffon, R.; Filho, U. P. R. Surface Organometallic Chemistry of Vanadium(V): Reactivity of (ButN□)VNp3 towards Silica. *J. Organomet. Chem.* **2001**, *625* (1), 101–107. https://doi.org/10.1016/S0022-328X(00)00908-6.
(27) Ruitenbeek, M.; van Dillen, A. J.; de Groot, F. M. F.; Wachs, I. E.; Geus, J. W.; Koningsberger, D. C. The Structure of Vanadium Oxide Species on γ-Alumina; an in Situ X-Ray Absorption Study during Catalytic Oxidation. *Top. Catal.* **2000**, *10* (3), 241–254. https://doi.org/10.1023/A:1019180504770.
(28) Weckhuysen, B. M.; Jehng, J.-M.; Wachs, I. E. In Situ Raman Spectroscopy of Supported Transition Metal Oxide Catalysts: 18O2−16O2 Isotopic Labeling Studies. *J. Phys. Chem. B* **2000**, *104* (31), 7382–7387. https://doi.org/10.1021/jp000055n.
(29) Tanaka, T.; Yamashita, H.; Tsuchitani, R.; Funabiki, T.; Yoshida, S. X-Ray Absorption (EXAFS/XANES) Study of Supported Vanadium Oxide Catalysts. Structure of Surface Vanadium Oxide Species on Silica and γ-Alumina at a Low Level of Vanadium Loading. *J. Chem. Soc. Faraday Trans. 1 Phys. Chem. Condens. Phases* **1988**, *84* (9), 2987–2999. https://doi.org/10.1039/F19888402987.
(30) Pelletier, J. D. A.; Basset, J.-M. Catalysis by Design: Well-Defined Single-Site Heterogeneous Catalysts. *Acc. Chem. Res.* **2016**, *49* (4), 664–677. https://doi.org/10.1021/acs.accounts.5b00518.
(31) Popoff, N.; Mazoyer, E.; Pelletier, J.; Gauvin, R. M.; Taoufik, M. Expanding the Scope of Metathesis: A Survey of Polyfunctional, Single-Site Supported Tungsten Systems for Hydrocarbon Valorization. *Chem. Soc. Rev.* **2013**, *42* (23), 9035–9054. https://doi.org/10.1039/C3CS60115C.
(32) Mazoyer, E.; Merle, N.; Mallmann, A. de; Basset, J.-M.; Berrier, E.; Delevoye, L.; Paul, J.-F.; Nicholas, C. P.; Gauvin, R. M.; Taoufik, M. Development of the First Well-Defined Tungsten Oxo Alkyl Derivatives Supported on Silica by SOMC: Towards a Model of WO3/SiO2 Olefin Metathesis Catalyst. *Chem. Commun.* **2010**, *46* (47), 8944–8946. https://doi.org/10.1039/C0CC02507K.

(33) Bouhoute, Y.; Garron, A.; Grekov, D.; Merle, N.; Szeto, K. C.; De Mallmann, A.; Del Rosal, I.; Maron, L.; Girard, G.; Gauvin, R. M.; Delevoye, L.; Taoufik, M. Well-Defined Supported Mononuclear Tungsten Oxo Species as Olefin Metathesis Pre-Catalysts. *ACS Catal.* **2014**, *4* (11), 4232–4241. https://doi.org/10.1021/cs501294j.

(34) Espinas, J.; Pelletier, J.; Szeto, K. C.; Merle, N.; Le Roux, E.; Lucas, C.; Mallmann, A. D.; Basset, J.-M.; Taoufik, M.; Thivolle-Cazat, J. Preparation and Characterization of Metallacalixarenes Anchored to a Mesoporous Silica SBA-15 LP as Potential Catalysts. *Microporous Mesoporous Mater.* **2014**, *188*, 77–85. https://doi.org/10.1016/j.micromeso.2013.12.031.

(35) Garron, A.; Stoffelbach, F.; Merle, N.; C. Szeto, K.; Thivolle-Cazat, J.; Basset, J.-M.; Norsic, S.; Taoufik, M. Improved Direct Production of 2,3-Dimethylbutenes and 3,3-Dimethylbutene from 2-Methylpropene on Tungsten Hydride Based Catalysts. *Catal. Sci. Technol.* **2012**, *2* (12), 2453–2455. https://doi.org/10.1039/C2CY20539D.

(36) Popoff, N.; Espinas, J.; Pelletier, J.; Szeto, K. C.; Thivolle-Cazat, J.; Delevoye, L.; Gauvin, R. M.; Taoufik, M. Design and Application of a Hybrid Material Featuring Well-Defined, Tuneable Grafting Sites for Supported Catalysis. *ChemCatChem* **2013**, *5* (7), 1971–1977. https://doi.org/10.1002/cctc.201200850.

(37) Popoff, N.; Szeto, K. C.; Merle, N.; Espinas, J.; Pelletier, J.; Lefebvre, F.; Thivolle-Cazat, J.; Delevoye, L.; De Mallmann, A.; Gauvin, R. M.; Taoufik, M. Enforcing Z-Selectivity in Olefin Metathesis through Use of Catalysts Grafted on Well-Defined Phenolic Hybrid Material. *Catal. Today* **2014**, *235*, 41–48. https://doi.org/10.1016/j.cattod.2014.02.036.

(38) Szeto, K. C.; Mazoyer, E.; Merle, N.; Norsic, S.; Basset, J.-M.; Nicholas, C. P.; Taoufik, M. Metallacyclobutane Substitution and Its Effect on Alkene Metathesis for Propylene Production over W–H/Al2O3: Case of Isobutene/2-Butene Cross-Metathesis. *ACS Catal.* **2013**, *3* (9), 2162–2168. https://doi.org/10.1021/cs400508v.

(39) Szeto, K. C.; Jones, Z. R.; Merle, N.; Rios, C.; Gallo, A.; Le Quemener, F.; Delevoye, L.; Gauvin, R. M.; Scott, S. L.; Taoufik, M. A Strong Support Effect in Selective Propane Dehydrogenation Catalyzed by Ga(i-Bu)3 Grafted onto γ-Alumina and Silica. *ACS Catal.* **2018**, *8* (8), 7566–7577. https://doi.org/10.1021/acscatal.8b00936.

(40) Szeto, K. C.; Loges, B.; Merle, N.; Popoff, N.; Quadrelli, A.; Jia, H.; Berrier, E.; De Mallmann, A.; Delevoye, L.; Gauvin, R. M.; Taoufik, M. Vanadium Oxo Organometallic Species Supported on Silica for the Selective Non-Oxidative Dehydrogenation of Propane. *Organometallics* **2013**, *32* (21), 6452–6460. https://doi.org/10.1021/om400795s.

(41) Love, A. M.; Carrero, C. A.; Chieregato, A.; Grant, J. T.; Conrad, S.; Verel, R.; Hermans, I. Elucidation of Anchoring and Restructuring Steps during Synthesis of Silica-Supported Vanadium Oxide Catalysts. *Chem. Mater.* **2016**, *28* (15), 5495–5504. https://doi.org/10.1021/acs.chemmater.6b02118.

(42) P. Högerl, M.; Goh, L. M. S.; Abou-Hamad, E.; Barman, S.; Dachwald, O.; Ahmad Pasha, F.; Pelletier, J.; Köhler, K.; D'Elia, V.; Cavallo, L.; Basset, J.-M. SOMC Grafting of Vanadium Oxytriisopropoxide (VO(O i Pr) 3) on Dehydroxylated Silica; Analysis of Surface Complexes and Thermal Restructuring Mechanism. *RSC Adv.* **2018**, *8* (37), 20801–20808. https://doi.org/10.1039/C8RA02419G.

(43) Barman, S.; Maity, N.; Bhatte, K.; Ould-Chikh, S.; Dachwald, O.; Haessner, C.; Saih, Y.; Abou-Hamad, E.; Llorens, I.; Hazemann, J. L.; Kohler, K.; D'Elia, V.; Basset, J. M. Single-Site VOx Moieties Generated on Silica by Surface Organometallic Chemistry: A Way To Enhance the Catalytic Activity in the Oxidative Dehydrogenation of Propane. *ACS Catal.* **2016**, *6* (9), 5908–5921. https://doi.org/10.1021/acscatal.6b01263.

(44) Schweitzer, N. M.; Hu, B.; Das, U.; Kim, H.; Greeley, J.; Curtiss, L. A.; Stair, P. C.; Miller, J. T.; Hock, A. S. Propylene Hydrogenation and Propane Dehydrogenation by a Single-Site Zn2+ on Silica Catalyst. *ACS Catal.* **2014**, *4* (4), 1091–1098. https://doi.org/10.1021/cs401116p.

(45) Hu, B.; Schweitzer, N. M.; Zhang, G.; Kraft, S. J.; Childers, D. J.; Lanci, M. P.; Miller, J. T.; Hock, A. S. Isolated FeII on Silica As a Selective Propane Dehydrogenation Catalyst. *ACS Catal.* **2015**, *5* (6), 3494–3503. https://doi.org/10.1021/acscatal.5b00248.
(46) Le Quéméner, F.; Barman, S.; Merle, N.; Aljuhani, M. A.; Samantaray, M. K.; Saih, Y.; Szeto, K. C.; De Mallmann, A.; Minenkov, Y.; Huang, K.-W.; Cavallo, L.; Taoufik, M.; Basset, J.-M. Metathetic Oxidation of 2-Butenes to Acetaldehyde by Molecular Oxygen Using the Single-Site Olefin Metathesis Catalyst (≡SiO)2Mo(═O)2. *ACS Catal.* **2018**, *8* (8), 7549–7555. https://doi.org/10.1021/acscatal.8b01767.
(47) Larabi, C.; Merle, N.; Le Quéméner, F.; Rouge, P.; Berrier, E.; Gauvin, R. M.; Le Roux, E.; de Mallmann, A.; Szeto, K. C.; Taoufik, M. New Synthetic Approach towards Well-Defined Silica Supported Tungsten Bis-Oxo, Active Catalysts for Olefin Metathesis. *Catal. Commun.* **2018**, *108*, 51–54. https://doi.org/10.1016/j.catcom.2018.01.031.
(48) Mathon, O.; Beteva, A.; Borrel, J.; Bugnazet, D.; Gatla, S.; Hino, R.; Kantor, I.; Mairs, T.; Munoz, M.; Pasternak, S.; Perrin, F.; Pascarelli, S. The Time-Resolved and Extreme Conditions XAS (TEXAS) Facility at the European Synchrotron Radiation Facility: The General-Purpose EXAFS Bending-Magnet Beamline BM23. *J. Synchrotron Radiat.* **2015**, *22*, 1548–1554. https://doi.org/10.1107/S1600577515017786.
(49) Ravel, B.; Newville, M. ATHENA, ARTEMIS, HEPHAESTUS: Data Analysis for X-Ray Absorption Spectroscopy Using IFEFFIT. *J. Synchrotron Radiat.* **2005**, *12* (4), 537–541. https://doi.org/10.1107/S0909049505012719.
(50) Basset, J.-M.; Baudouin, A.; Bayard, F.; Candy, J.-P.; Copéret, C.; De Mallmann, A.; Godard, G.; Kuntz, E.; Lefebvre, F.; Lucas, C.; Norsic, S.; Pelzer, K.; Quadrelli, A.; Santini, C.; Soulivong, D.; Stoffelbach, F.; Taoufik, M.; Thieuleux, C.; Thivolle-Cazat, J.; Veyre, L. Preparation of Single Site Catalysts on Oxides and Metals Prepared via Surface Organometallic Chemistry. In *Modern Surface Organometallic Chemistry*; John Wiley & Sons, Ltd, 2009; pp 23–73. https://doi.org/10.1002/9783527627097.ch2.
(51) Conte, P.; Spaccini, R.; Piccolo, A. State of the Art of CPMAS 13C-NMR Spectroscopy Applied to Natural Organic Matter. *Prog. Nucl. Magn. Reson. Spectrosc.* **2004**, *44* (3–4), 215–223.
(52) Bini, F.; Rosier, C.; Saint-Arroman, R. P.; Neumann, E.; Dablemont, C.; de Mallmann, A.; Lefebvre, F.; Niccolai, G. P.; Basset, J.-M.; Crocker, M.; Buijink, J.-K. Surface Organometallic Chemistry of Titanium: Synthesis, Characterization, and Reactivity of (⋮Si−O)NTi(CH2C(CH3)3)4-n (n = 1, 2) Grafted on Aerosil Silica and MCM-41. *Organometallics* **2006**, *25* (15), 3743–3760. https://doi.org/10.1021/om050675g.
(53) Hu, J. Z.; Xu, S.; Li, W.-Z.; Hu, M. Y.; Deng, X.; Dixon, D. A.; Vasiliu, M.; Craciun, R.; Wang, Y.; Bao, X.; Peden, C. H. F. Investigation of the Structure and Active Sites of TiO2 Nanorod Supported VOx Catalysts by High-Field and Fast-Spinning 51V MAS NMR. *ACS Catal.* **2015**, *5* (7), 3945–3952. https://doi.org/10.1021/acscatal.5b00286.
(54) McGregor, J. Solid-State NMR of Oxidation Catalysts. *Met. Oxide Catal.* **2008**, 195–242.
(55) Rice, G. L.; Scott, S. L. Characterization of Silica-Supported Vanadium(V) Complexes Derived from Molecular Precursors and Their Ligand Exchange Reactions. *Langmuir* **1997**, *13* (6), 1545–1551. https://doi.org/10.1021/la960679d.
(56) Catana, G.; Rao, R. R.; Weckhuysen, B. M.; Van Der Voort, P.; Vansant, E.; Schoonheydt, R. A. Supported Vanadium Oxide Catalysts: Quantitative Spectroscopy, Preferential Adsorption of V4+/5+, and Al2O3 Coating of Zeolite Y. *J. Phys. Chem. B* **1998**, *102* (41), 8005–8012. https://doi.org/10.1021/jp981482s.
(57) Gao, X.; Wachs, I. E. Investigation of Surface Structures of Supported Vanadium Oxide Catalysts by UV−vis−NIR Diffuse Reflectance Spectroscopy. *J. Phys. Chem. B* **2000**, *104* (6), 1261–1268. https://doi.org/10.1021/jp992867t.
(58) Wegener, S. L.; Kim, H.; Marks, T. J.; Stair, P. C. Precursor Nuclearity Effects in Supported Vanadium Oxides Prepared by Organometallic Grafting. *J. Phys. Chem. Lett.* **2011**, *2* (3), 170–175. https://doi.org/10.1021/jz101490p.

(59) Wong, J.; Lytle, F. W.; Messmer, R. P.; Maylotte, D. H. K-Edge Absorption Spectra of Selected Vanadium Compounds. *Phys. Rev. B* **1984**, *30* (10), 5596–5610. https://doi.org/10.1103/PhysRevB.30.5596.
(60) Nabavi, M.; Taulelle, F.; Sanchez, C.; Verdaguer, M. Xanes and 51V Nmr Study of Vanadium-Oxygen Compounds. *J. Phys. Chem. Solids* **1990**, *51* (12), 1375–1382. https://doi.org/10.1016/0022-3697(90)90020-G.
(61) Chaurand, P.; Rose, J.; Briois, V.; Salome, M.; Proux, O.; Nassif, V.; Olivi, L.; Susini, J.; Hazemann, J.-L.; Bottero, J.-Y. New Methodological Approach for the Vanadium K-Edge X-Ray Absorption Near-Edge Structure Interpretation: Application to the Speciation of Vanadium in Oxide Phases from Steel Slag. *J. Phys. Chem. B* **2007**, *111* (19), 5101–5110. https://doi.org/10.1021/jp063186i.
(62) Keller, D. E.; Visser, T.; Soulimani, F.; Koningsberger, D. C.; Weckhuysen, B. M. Hydration Effects on the Molecular Structure of Silica-Supported Vanadium Oxide Catalysts: A Combined IR, Raman, UV–Vis and EXAFS Study. *Vib. Spectrosc.* **2007**, *43* (1), 140–151. https://doi.org/10.1016/j.vibspec.2006.07.005.
(63) Nguyen, L. D.; Loridant, S.; Launay, H.; Pigamo, A.; Dubois, J. L.; Millet, J. M. M. Study of New Catalysts Based on Vanadium Oxide Supported on Mesoporous Silica for the Partial Oxidation of Methane to Formaldehyde: Catalytic Properties and Reaction Mechanism. *J. Catal.* **2006**, *237* (1), 38–48. https://doi.org/10.1016/j.jcat.2005.10.016.
(64) Lewandowska, A. E.; Banares, M. A.; Tielens, F.; Che, M.; Dzwigaj, S. Different Kinds of Tetrahedral V Species in Vanadium-Containing Zeolites Evidenced by Diffuse Reflectance UV−vis, Raman, and Periodic Density Functional Theory. *J. Phys. Chem. C* **2010**, *114* (46), 19771–19776. https://doi.org/10.1021/jp107589d.
(65) Liu, Y.-M.; Cao, Y.; Yi, N.; Feng, W.-L.; Dai, W.-L.; Yan, S.-R.; He, H.-Y.; Fan, K.-N. Vanadium Oxide Supported on Mesoporous SBA-15 as Highly Selective Catalysts in the Oxidative Dehydrogenation of Propane. *J. Catal.* **2004**, *224* (2), 417–428. https://doi.org/10.1016/j.jcat.2004.03.010.
(66) Luca, V.; Thomson, S.; Howe, R. F. Spectroscopic Investigation of Vanadium Speciation Invanadium-Doped Nanocrystalline Anatase. *J. Chem. Soc. Faraday Trans.* **1997**, *93* (12), 2195–2202. https://doi.org/10.1039/A608569E.
(67) Keränen, J.; Auroux, A.; Ek, S.; Niinistö, L. Preparation, Characterization and Activity Testing of Vanadia Catalysts Deposited onto Silica and Alumina Supports by Atomic Layer Deposition. *Appl. Catal. Gen.* **2002**, *228* (1), 213–225. https://doi.org/10.1016/S0926-860X(01)00975-9.
(68) Das, N.; Eckert, H.; Hu, H.; Wachs, I. E.; Walzer, J. F.; Feher, F. J. Bonding States of Surface Vanadium (V) Oxide Phases on Silica: Structural Characterization by Vanadium-51 NMR and Raman Spectroscopy. *J. Phys. Chem.* **1993**, *97* (31), 8240–8243.
(69) Feher, F. J.; Walzer, J. F. Synthesis and Characterization of Vanadium-Containing Silsesquioxanes. *Inorg. Chem.* **1991**, *30* (8), 1689–1694. https://doi.org/10.1021/ic00008a005.
(70) Jaegers, N. R.; Wan, C.; Hu, M. Y.; Vasiliu, M.; Dixon, D. A.; Walter, E.; Wachs, I. E.; Wang, Y.; Hu, J. Z. Investigation of Silica-Supported Vanadium Oxide Catalysts by High-Field 51V Magic-Angle Spinning NMR. *J. Phys. Chem. C* **2017**, *121* (11), 6246–6254. https://doi.org/10.1021/acs.jpcc.7b01658.
(71) Miller, J. M.; Lakshmi, L. J. V2O5 Catalysts Supported on Al2O3–SiO2 Mixed Oxide: 51V, 1H MAS Solid-State NMR, DRIFTS and Methanol Oxidation Studies. *Appl. Catal. Gen.* **2000**, *190* (1), 197–206. https://doi.org/10.1016/S0926-860X(99)00296-3.
(72) Grant, J. T.; Carrero, C. A.; Love, A. M.; Verel, R.; Hermans, I. Enhanced Two-Dimensional Dispersion of Group V Metal Oxides on Silica. *ACS Catal.* **2015**, *5* (10), 5787–5793. https://doi.org/10.1021/acscatal.5b01679.
(73) McGregor, J. Solid-State NMR of Oxidation Catalysts. In *Metal Oxide Catalysis*; John Wiley & Sons, Ltd, 2008; pp 195–242. https://doi.org/10.1002/9783527626113.ch5.

(74) Das, N.; Eckert, H.; Hu, H.; Wachs, I. E.; Walzer, J. F.; Feher, F. J. *Bonding states of surface vanadium(V) oxide phases on silica: structural characterization by vanadium-51 NMR and Raman spectroscopy*. ACS Publications. https://pubs.acs.org/doi/pdf/10.1021/j100133a020 (accessed 2022-05-17). https://doi.org/10.1021/j100133a020.
(75) Terry, K. W.; Lugmair, C. G.; Tilley, T. D. Tris(Tert-Butoxy)Siloxy Complexes as Single-Source Precursors to Homogeneous Zirconia- and Hafnia-Silica Materials. An Alternative to the Sol-Gel Method. *J. Am. Chem. Soc.* **1997**, *119* (41), 9745–9756. https://doi.org/10.1021/ja971405v.
(76) Niccolai, G. P.; Basset, J.-M. Primary Selectivity in the Activation of the Carbon-Hydrogen Bonds of Propane by Silica Supported Zirconium Hydride. *Appl. Catal. Gen.* **1996**, *146* (1), 145–156. https://doi.org/10.1016/0926-860X(96)00120-2.
(77) C. Szeto, K.; Hardou, L.; Merle, N.; Basset, J.-M.; Thivolle-Cazat, J.; Papaioannou, C.; Taoufik, M. Selective Conversion of Butane into Liquid Hydrocarbon Fuels on Alkane Metathesis Catalysts. *Catal. Sci. Technol.* **2012**, *2* (7), 1336–1339. https://doi.org/10.1039/C2CY20150J.
(78) Olsbye, U.; Virnovskaia, A.; Prytz, Ø.; Tinnemans, S.; Weckhuysen, B. Mechanistic Insight in the Ethane Dehydrogenation Reaction over Cr/Al2O3 Catalysts. *Catal. Lett.* **2005**, *103*, 143–148. https://doi.org/10.1007/s10562-005-6521-7.
(79) Harlin, M. E.; Niemi, V. M.; Krause, A. O. I. Alumina-Supported Vanadium Oxide in the Dehydrogenation of Butanes. *J. Catal.* **2000**, *195* (1), 67–78. https://doi.org/10.1006/jcat.2000.2969.
(80) Chen, S.; Qin, Z.; Wang, G.; Dong, M.; Wang, J. Promoting Effect of Carbon Dioxide on the Dehydrogenation of Ethylbenzene over Silica-Supported Vanadium Catalysts. *Fuel* **2013**, *109*, 43–48. https://doi.org/10.1016/j.fuel.2012.06.004.

TOC:

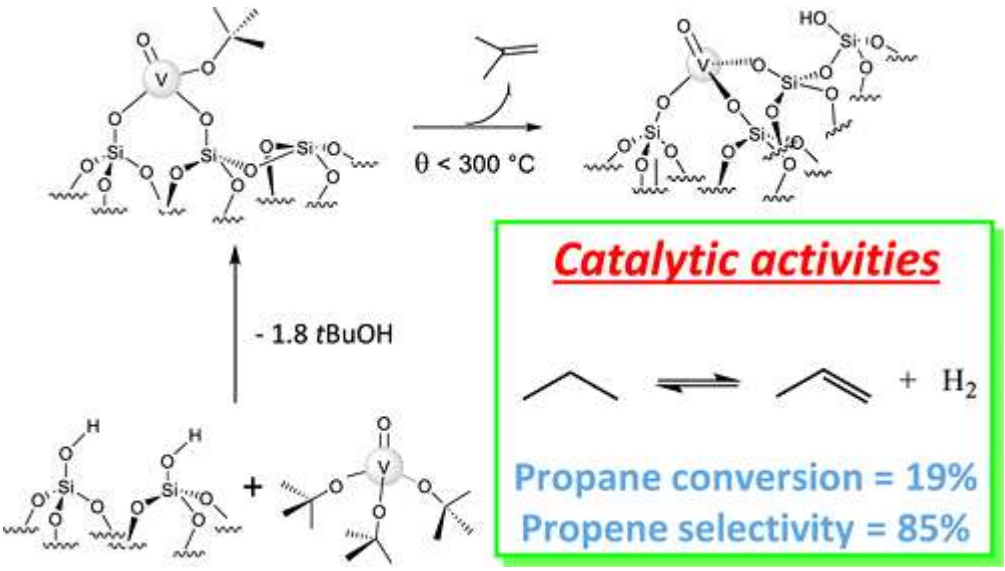

Preparation of tripodal Vanadium Oxo-Organometallic Species Supported on Silica, $[(\equiv SiO)_3V(=O)]$, for Selective Non-Oxidative Dehydrogenation of Propane

Abou Nakad Jessy,[a] Rajapaksha Remy,[a] Szeto Kai C.,[a] De Mallmann Aimery,[a] Taoufik Mostafa[a,*]

[a] Université Lyon 1, Institut de Chimie Lyon, CPE Lyon, CNRS, UMR 5128 CP2M, 43 Bd du 11 Novembre 1918, F-69616 Villeurbanne Cedex, France. E-mail: Mostafa.Taoufik@univ-lyon1.fr; Fax: +33 (0)472 431 798; Tel: +33 (0)472 431 795

Supporting information

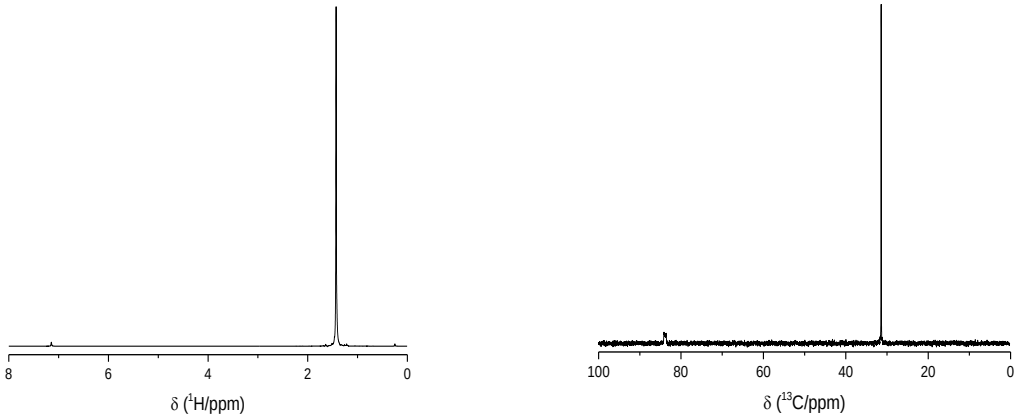

Figure S1. NMR spectra of $[V(=O)(OtBu)_3]$ molecular complex: Left: ^{1}H (d_1=1 s) and Right: ^{13}C $\{^{1}H\}$ (d_1=10 s).

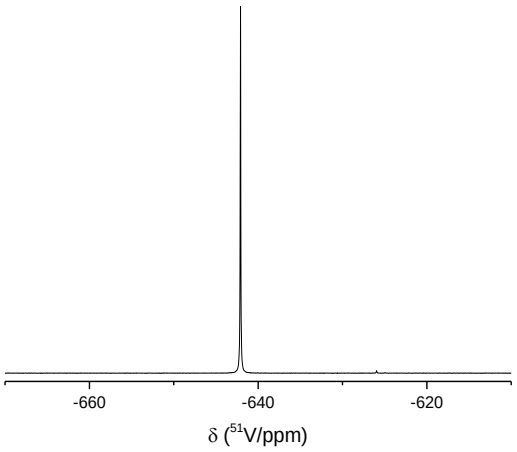

Figure S2. ^{51}V NMR spectrum of [V(=O)(O*t*Bu)$_3$] molecular complex (d_1= 1s).

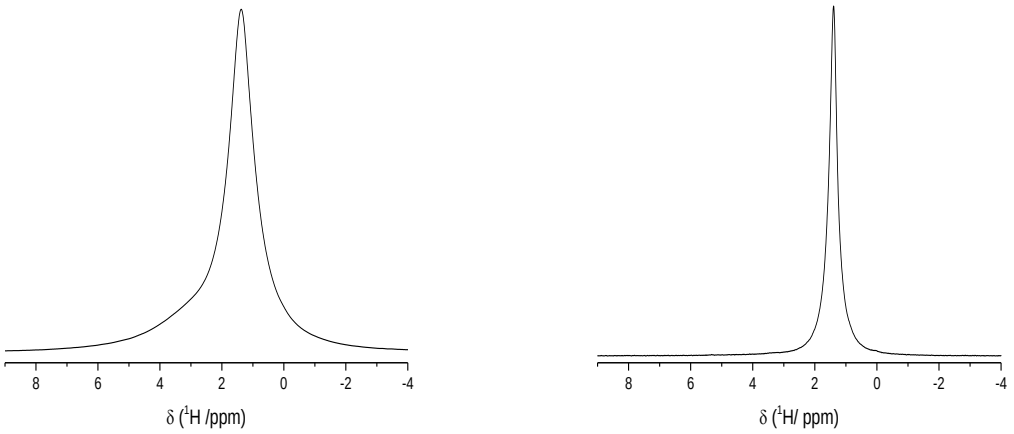

Figure S3. ^1H MAS NMR spectra, **Left**: V(=O)(O*t*Bu)$_3$/SiO$_{2\text{-}200}$ and **Right**: V(=O)(O*t*Bu)$_3$/SiO$_{2\text{-}700}$ (11.8 T, 10 kHz MAS, d_1= 5 s)

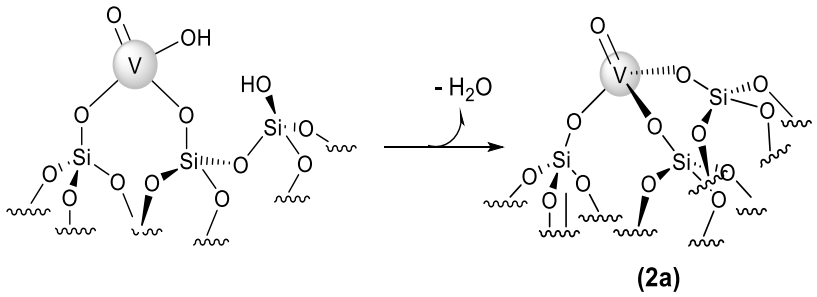

Scheme S1. Partial condensation of V-OH with the remaining silanols, leading to the formation of tripodal V oxo and water

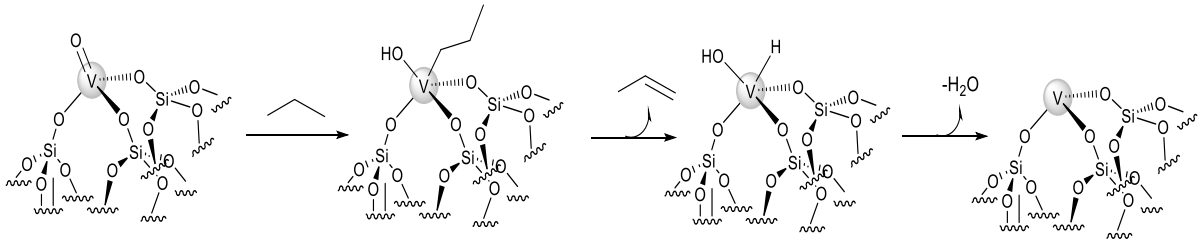

Scheme S2. Formation of tripodal active species after activation of propane and release of water

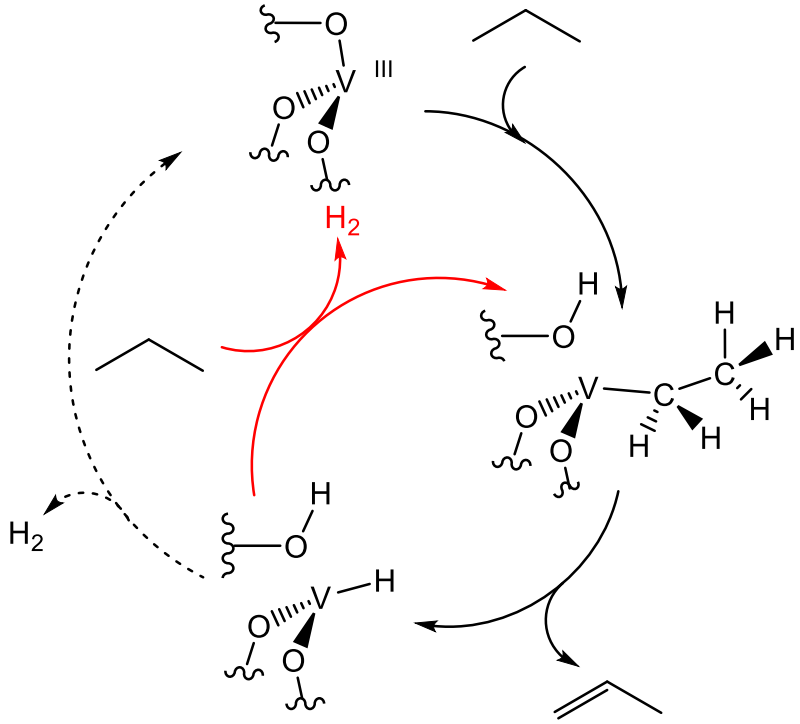

Scheme S3. Proposed mechanism for propane dehydrogenation based on V